AD-A235 016

(2)

REPORT DOCUMENTATION PAGE

Unclassified	1b. RESTRICTIVE MARKINGS
2a. SECURITY CLASSIFICATION AUTHORITY	3. DISTRIBUTION / AVAILABILITY OF REPORT: unlimited
2b. DECLASSIFICATION / DOWNGRADING SCHEDULE	
4. PERFORMING ORGANIZATION REPORT NUMBER(S): MEMS-ALC-14	5. MONITORING ORGANIZATION REPORT NUMBER(S): Air Force Office of Scientific Research
6a. NAME OF PERFORMING ORGANIZATION: Carnegie Mellon University; 6b. OFFICE SYMBOL (If applicable)	7a. NAME OF MONITORING ORGANIZATION: Air Force Office of Scientific Research
6c. ADDRESS (City, State, and ZIP Code): Dept. of Metall. Eng. & Materials Science, Carnegie Mellon University, Pittsburgh, PA 15213	7b. ADDRESS (City, State, and ZIP Code): Bolling AFB, Bldg. 410, Washington, DC 20332
8a. NAME OF FUNDING / SPONSORING ORGANIZATION: AFOSR; 8b. OFFICE SYMBOL (If applicable): NE	9. PROCUREMENT INSTRUMENT IDENTIFICATION NUMBER: AFOSR 90-0033
8c. ADDRESS (City, State, and ZIP Code): Bolling AFB, Bldg. 410, Washington, DC 20332	10. SOURCE OF FUNDING NUMBERS: PROGRAM ELEMENT NO. 61102F; PROJECT NO. 2306; TASK NO. A1; WORK UNIT ACCESSION NO

11. TITLE (Include Security Classification)
Fundamentals of Mechanical Behavior in Intermetallic Compounds

12. PERSONAL AUTHOR(S)
Howe, James M. and Thompson, Anthony W.

13a. TYPE OF REPORT	13b. TIME COVERED	14. DATE OF REPORT (Year, Month, Day)	15. PAGE COUNT
Annual	FROM 10-1-89 TO 9-30-90	1 February 1991	48

16. SUPPLEMENTARY NOTATION

17. COSATI CODES			18. SUBJECT TERMS (Continue on reverse if necessary and identify by block number)
FIELD	GROUP	SUB-GROUP	

19. ABSTRACT (Continue on reverse if necessary and identify by block number)

Research in the first year of this program has examined mechanical behavior and creep of titanium aluminide alloys, both based on Ti_3Al and TiAl, with the goal being better understanding of relationships between microstructure and mechanical properties of these intermetallic compound-based alloys. Detailed microstructural characterization has been conducted for both types of aluminide alloys. For Ta additions to TiAl alloys, which are thought to improve ductility, lowered stacking fault energy and increased twinning have been found. For a Ti_3Al-based alloy, detailed stress and temperature dependences of creep have been measured, and a strong microstructural dependence of creep properties has been established.

UNCLASSIFIED

20. DISTRIBUTION / AVAILABILITY OF ABSTRACT	21. ABSTRACT SECURITY CLASSIFICATION
☒ UNCLASSIFIED/UNLIMITED ☐ SAME AS RPT ☐ DTIC USERS	

22a. NAME OF RESPONSIBLE INDIVIDUAL	22b TELEPHONE (Include Area Code)	22c. OFFICE SYMBOL
R. Rosenstein	202-767-4933	NE

DD FORM 1473, 84 MAR — 83 APR edition may be used until exhausted. All other editions are obsolete. SECURITY CLASSIFICATION OF THIS PAGE

91

FUNDAMENTALS OF MECHANICAL BEHAVIOR IN INTERMETALLIC COMPOUNDS

ANNUAL REPORT
1 OCTOBER 1989 - 30 SEPTEMBER 1990

Air Force Office of Scientific Research

Grant AFOSR-90-0033
(CMU Account 1-52159)

A-1

J.M. Howe and A.W. Thompson
Principal Investigators

Dept. of Metallurgical Engineering and Materials Science
Carnegie Mellon University

Report No. MEMS-ALC-14
1 February 1991

TABLE OF CONTENTS

Fundamentals of Mechanical Behavior in Intermetallic Compounds

ANNUAL REPORT

Abstract

Research in the first year of this program has examined mechanical behavior and creep of titanium aluminide alloys, based on both Ti_3Al and TiAl, with the goal being better understanding of relationships between microstructure and mechanical properties of these intermetallic compound-based alloys. Detailed microstructural characterization has been conducted for both types of aluminide alloys. For Ta additions to TiAl alloys, which are thought to improve ductility, lowered stacking fault energy and increased twinning has been found. For a Ti_3Al-base alloy, detailed stress and temperature dependences of creep have been measured, and a strong microstructural dependence of creep properties has been established.

Background

This is the first annual report on the subject program. The experimental materials for this research are intermetallic compounds based on titanium and aluminum, with some initial work on the established alloys of the α_2 family (Ti_3Al), but with a focus on advanced alloys based on TiAl and $TiAl_3$. The goal of the work is to advance fundamental understanding of the performance of these alloys, particularly their mechanical behavior, with the preliminary work on α_2 alloys serving as a model system for behavior of these intermetallic compounds. There is already ample evidence that properties and performance of these alloys depend on both processing variables and on metallurgical variables such as microstructure. We are particularly interested in the behavior of the interfaces in the multi-phase microstructures of these alloys, because of indications that the properties, especially fracture properties, are sensitively dependent on interfacial performance. One means of examining these interfaces is with the tool of Atomic Resolution Microscopy (ARM), using the JEOL 4000EX facilities for ARM at Carnegie Mellon.

For this initial year, Prof. Howe and his post-doctoral associate, J.R. Singh, have made extensive observations on TiAl alloys, including several publications, and those results are presented below in some detail. In addition, completion of experimental work on creep of the alloy Ti-24-11, based on α_2, has been accomplished by graduate student Diane E. Albert with A.W. Thompson.

During the past year, the program has been conducted by both investigators at Carnegie Mellon, but with the move of J.M. Howe to Virginia, work during most of the next fiscal year will be conducted under a sub-contract to the University of Virginia.

TECHNICAL PROGRESS REPORT

1 October 1989 - 30 September 1990

CREEP OF AN ALPHA-2 TITANIUM ALUMINIDE ALLOY

Diane E. Albert, Graduate Student
Anthony W. Thompson, Principal Investigator

First-year work

Experimental work has been completed on creep behavior of Ti-24 Al-11 Nb (atomic %), called Ti-24-11 below. This alloy is based on Ti_3Al, designated α_2 in the Ti-Al phase diagram, and was among the first α_2 alloys accepted for use. These experiments have shown clearly that the material's microstructure exerts a profound influence on creep behavior, as has also been shown for a similar α_2 alloy, Ti-25 Al-10 Nb-3 V-1 Mo [1]. At the highest temperatures, there are some indirect indications of interphase boundary sliding in Ti-24-11, and accordingly the more elongated, coarse microstructures provide the best creep resistance. It is essential, however, that such coarse microstructures not comprise colonies of parallel α_2 plates, but instead should be of the so-called "basketweave" structure, made up of individual α_2 plates of differing orientation, since the plates within colonies share a common crystallographic orientation and thus act as a larger slip unit during creep. At intermediate temperatures, near 650°C, some aspects of low-temperature deformation behavior continue to be effective, and microstructural refinement, deleterious at high temperatures, offers improvements in some kinds of structures.

Measurements at several stresses and temperatures made possible determination of the stress and temperature dependence of creep behavior in this alloy, as a function of microstructure. The stress dependence, expressed through the so-called "stress exponent" n [2], was typically near or somewhat less than $n = 4$, with a tendency toward lower values of n as temperature increased. This trend toward lower values is often taken to indicate an increased diffusional contribution to creep, particularly when boundary sliding comes into play. The temperature dependence can be expressed as the apparent activation energy, which in simple microstructures is expected to be near the value of the activation energy for self-diffusion [2]. In Ti-24-11, or for that matter in Ti_3Al, the self-diffusion parameters are not known. Work to date, however, seems to indicate that the apparent creep activation energy can vary over a considerable range, from above 300 kJ/mol at higher stresses, e.g. 100 MPa or more [1], to values near 120 kJ/mol when applied stresses are lower [3,4]. More work will be needed to identify unambiguously the operative creep

mechanisms in these regimes of stress and temperature, but a considerable base of experimental knowledge has been accomplished on the α_2 alloys to date.

Listed at the end of this section are the AFOSR-sponsored publications of the past year. Attached is a copy of number 3, as an overview of the creep work on Ti-24-11.

References

1. W. Cho, A.W. Thompson and J.C. Williams, "Creep of Ti-25 Al-10 Nb-3 V-1 Mo", *Metall. Trans. A*, 1990, vol. 21A, pp. 641-651.
2. H.M. Frost and M.F. Ashby, *Deformation Mechanism Maps: The Plasticity and Creep of Metals and Ceramics*, Pergamon Press, Oxford, England, 1982, pp.11-14.
3. D. E. Albert and A. W. Thompson, "Creep Behavior of Ti-24 Al-11 Nb," in *Microstructure/Property Relationships in Titanium Alloys and Titanium Aluminides*, Y.-W. Kim, R.R. Boyer and J.A. Hall, eds., TMS-AIME, Warrendale, PA, in press.
4. A.W. Thompson and T.M. Pollock, "Creep of $\alpha_2 + \beta$ Titanium Aluminide Alloys," *ISIJ Internt. Jnl.*, in press.

Plans for second year

A new graduate student, Mrs. Kezhong Li, has joined the program and will be beginning work on mechanical properteis of TiAl and $TiAl_3$ alloys.

AFOSR-supported Publications

1. R.F. Buck and A.W. Thompson, "Environmental Fatigue in Al-SiC Composites," in *Environmental Effects on Advanced Materials*, R.E. Ricker and R.H. Jones, eds., TMS-AIME, Warrendale, PA, in press.
2. A.W. Thompson and R.F. Buck, "Fatigue Crack Growth Behavior of SiC-Reinforced Aluminum-Alloy Composites in Aggressive Environments," *Proc. 8th Internat. Conf. on Composite Materials*, G. Springer and S. Tsai, eds., SAMPE, Covina, CA, submitted.
3. D.E. Albert and A.W. Thompson, "Creep Behavior of Ti-24 Al-11 Nb," in *Microstructure/Property Relationships in Titanium Alloys and Titanium Aluminides*, R.R. Boyer and J.A. Hall, eds., TMS-AIME, Warrendale, PA, in press.
4. A.W. Thompson and T.M. Pollock, "Creep of $\alpha_2 + \beta$ Titanium Aluminide Alloys," *ISIJ Internat. Jnl.*, in press.
5. D.E. Albert and A.W. Thompson, "Microstructure Dependence of Creep in Ti-24-11", *Scripta Metall. Mater.*, submitted.

Presentations during first year

1. D. Albert and A.W. Thompson, "Microstructure and Creep Behavior of Ti-24-11," Symposium on Creep, Fatigue and Fracture of Titanium Aluminides, Fall Meeting, TMS-AIME, Indianapolis, IN, 3 Oct. 1989.
2. A.W. Thompson, "Creep of Alpha-2 Titanium Aluminides" (invited), Symposium on Titanium Aluminides, Aeromat '90, Long Beach, CA, 22 May 1990.
3. D.E. Albert and A.W. Thompson, "Creep Behavior of Ti-24 Al-11 Nb," Symposium on Microstructure/Property Relationships in Titanium Alloys and Titanium Aluminides, TMS-AIME Fall Meeting, Detroit, MI, 9 Oct. 1990.
4. R.F. Buck and A.W. Thompson, "Environmental Fatigue in Al-SiC Composites," Symposium on Environmental Effects on Advanced Materials, TMS-AIME Fall Meeting, Detroit, MI, 10 Oct. 1990.

CREEP BEHAVIOR OF Ti-24AL-11NB

Diane E. Albert and Anthony W. Thompson
Department of Metallurgical Engineering and Materials Science
Carnegie Mellon University, Pittsburgh, Pa. 15213

Introduction

The steady state creep behavior of the titanium aluminide Ti-24Al-11Nb has been investigated. The steady state creep rate as a function of stress and as a function of temperature was determined for four microstructures derived from this alloy. Test temperatures ranged from 650°C to 870°C and test stresses ranged from 15 MPa to 175 MPa. The apparent activation energy for creep, Q_c, was determined for three microstructures in the low stress regime. It is proposed to determine the type of mechanism controlling creep behavior in these materials in these stress and temperature regimes and to determine what effect microstructural features have on steady state creep rates.

Experimental Procedures

The Ti-24Al-11Nb material was received from the RMI Company, Niles, Ohio in the form of 1.25 cm thick cross-rolled plate. Thermomechanical processing of the material at RMI involved hot rolling, annealing at 1038°C for one hour and subsequent air cooling. The chemical composition is shown in Table I and the as-received (AR) microstructure is shown in Figure 1a. This microstructure is a relatively equiaxed α_2 morphology with very little of a second phase present as a film between the α_2 regions. This second phase is either a BCC type ß phase or ordered BCC, designated $ß_o$.(1,2) Blanks approximately 1.25 cm square and 10 cm long were cut by bandsaw from this as-received material; heat treatment and machining into cylindrical creep specimens followed.

TABLE I
Chemical Composition of Cross-Rolled Ti-24Al-11Nb Plate.

Al	Nb	Fe	O	C	H	Ti
24.6	10.5	0.068	0.161	0.039	0.02	bal (at%)
14.0	20.6	0.08	0.054	0.01	4.8×10^{-5}	bal (wt%)

Three heat treatments were selected to produce three microstructures. Solutionizing in the ß phase field at 1200°C for one hour then air cooling produced fine acicular α_2 plates arranged in a Widmanstätten basketweave morphology, as shown in Figure 1b. Solutionizing at 1200°C for one hour with a subsequent α_2+ß phase field (1000°C) solutionizing for 15 minutes and air cool resulted in a fine Widmanstätten basketweave morphology with primary and secondary acicular α_2 plates as seen in Figure 1c. Holding for 30 minutes at 1000°C resulted in α_2 plate coarsening, as seen in Figure 1d.

An analysis of the effect which microstructural features have on steady state creep rate is possible by comparing creep behavior of selected specimens. Comparing creep rate differences between the materials held at 1000°C for 15 minutes and 30 minutes allows a determination of the effect of α_2 plate size on creep, as the degree of α_2 plate coarseness is the only microstructural variable. Since there is more α_2 present, there will be some depletion of the ß phase in α-stabilizing elements, but there is such a relatively small amount of ß present in the first place, it is assumed that this effect is negligible. The α_2 plate size of the 1200AC and 1000AC-15 is very similar; however the 1000AC-15 material will have a decreased amount of $ß_o$ phase and a corresponding increase in amount of α_2 phase present. The morphology of the as-received microstructure is roughly equiaxed α_2, not acicular, basketweave α_2. Evidence of texture is supported by the presence of elongated, aligned α_2.

The specimen used in the high-temperature constant-load creep tests was of a typical cylindrical configuration. A groove between the threads and the gage length on each end of the specimen allows for extensometer placement. Sufficient material was removed from the blank after exposure to high temperatures to ensure no oxygen-enriched material remained. Constant temperature creep tests were conducted at 650°C, 760°C, and 870°C in air, under decreasing tensile stresses. Single lever creep frames with a load ratio of 20:1 were used in all tests. Steady state creep rate *vs.* temperature tests were conducted at 100 MPa and 31.38 MPa to determine the apparent activation energy of creep. Creep strain was measured using an extensometer and a SLVC transducer which allowed a strain resolution of 5×10^{-6}. During creep tests, specimen temperatures were monitored continuously with type-K thermocouples attached to the gage length. Temperature variation during the tests was not greater than 2° C.

Results and Discussion

The results of steady state creep rate *vs.* stress tests for each microstructure at the three temperatures are shown in Figures 2, 3, and 4. For materials which undergo power-law creep, plotting $\log \dot{\varepsilon}_s$ *vs.* $\log \sigma$ will result in a straight line with a slope equal to **n**, the power law exponent.(3-6) It is seen that the as-received microstructure has the poorest resistance to creep at all temperatures. At both 650°C and 760°C, note that the 1200AC and 1000AC-15 structures have almost identical creep rates with 1000AC-30 displaying a superior creep rate. At 870°C, however, the creep resistance of 1000AC-15 is seen to be superior to both 1200AC and 1000AC-30, except at high stresses where 1000AC-30 has slightly better creep resistance. Duplication of tests confirmed these trends.

In Figure 5, each microstructure's creep behavior at each of the three test temperatures are plotted together on one graph. The slope, **n**, of each curve is indicated. In all cases, an increase in test temperature leads to a decrease in the value of **n** in the high stress region. At lower temperatures and lower stresses, 1000AC-30, AR, and 1200AC structures display a change in slope and ostensibly a change in creep mechanism. At high stresses, the value of **n** is large; at low stresses the slope is much less steep. Higher values of **n** (3 to 10) indicate dislocation glide and climb processes (7,8); a value of **n**=1 indicates diffusional creep by a stress-directed flow of atoms with grain boundaries acting as sources and sinks. This process occurs at low to intermediate stresses ($\sigma = 10^{-5}$ to 10^{-4})E where E is the Young's modulus.(9,10) A value of **n**=2 indicates grain (or phase) boundary sliding mechanisms. (11) The low stress slopes of these materials approximate the slope of the curves at high temperatures, where diffusion processes are dominant.

In Figure 6, the results of steady state creep rate *vs.* temperature tests are shown. Again, assuming power law creep, when $\log \dot{\varepsilon}_s$ *vs.* 1/T is plotted, a straight line with a slope

equal to Q_c, the apparent activation energy of creep, results. A creep activation energy of 206 kJ/mol for stoichiometric Ti_3Al at all stresses and temperatures has been measured.(12) Widmanstätten basketweave Ti-25-10-3-1 in the climb-controlled creep regime was found to have a Q_c of 305 kJ/mol.(13) The activation energy in the low stress regime for Ti-24-11 with a 100% transformed ß microstructure was determined to be 120 kJ.(1) It is thought that the apparent activation energies for high temperature creep in metals are independent of creep stress and strain,(14) but different mechanisms seem to be dominant in different stress regimes. In this work, the AR microstructure had an average Q_c of 110 kJ/mol; the 1000AC-15, 142 kJ/mol; and the 1200AC structure, a value of 134 kJ/mol. All values were measured in the low stress regime, and are in fairly good agreement with the value of 121 kJ/mol for grain boundary diffusion in fine-grained α titanium at low stresses.(15) It has been suggested that the activation energy for both crystallographic slip and grain boundary sliding are the same and that slip controls sliding.(16)

Discussion

Recrystallization and grain growth during creep, α plate width, ß volume fraction, and α/α *vs.* ß/ß boundaries are all factors that are thought to influence steady-state creep rate in conventional titanium alloys.(17) If only plate size is considered to control steady state creep rate in titanium aluminides, then we would expect the microstructure with the smallest plates, that is, the 1200AC and 1000AC-15 structures, to have the best creep resistance, due to their short slip length. It is seen, however, that 1000AC-30 has superior creep resistance up to 870°C. Therefore, slip distance and corresponding dislocation motion within plates is not the sole controlling factor in creep in the temperature and stress range studied. Rather, since the 1000AC-30 plates are coarser than the plates present in 1000AC-15 and 1200AC, then it is true that there is less interphase boundary per unit area in this structure. The ratio $\varepsilon_{gb}/\varepsilon_t$, the strain due to grain boundary sliding to the total creep strain, was found to increase with increasing temperatures(16) or decreasing stresses(18). Also, the 1000AC structures should contain smaller amounts of $ß_o$ phase. This phase has a higher diffusion rate and thus, inferior creep resistance. This would explain the fact that 1000AC structures creep more slowly than the 1200AC structure. Examination of microstructures in crept specimens demonstrated that recrystallization and grain growth did not occur appreciably during creep. The presence of crystallographic texture, i.e. perhaps an alignment in basal planes, in the as-received material could help explain its high steady state creep rate.

Conclusions

Steady state creep rates as functions of stress and temperature of selected microstructural variants of Ti-24Al-11Nb were determined. The as-received (AR) microstructure was found to possess the poorest creep resistance at all temperatures, possibly due to texture. The 1000AC-30 microstructure possessed superior creep resistance at all stresses when tested at low temperatures. The 1000AC-15 microstructure had superior creep resistance only in the low stress regime at 870°C. For each structure, increasing temperature caused a decrease in the value of n in the high stress region. If a slope change occurred, the value of n in the low stress region was found to be close to unity, indicative of boundary sliding mechanisms. The apparent activation energy of creep for all microstructures was found to be 142 kJ/mol, 140 kJ/mol, and 115 kJ/mol for 1000AC-15, 1200AC and AR respectively. These values are very similar to the activation energy obtained for grain boundary diffusion in pure titanium. This evidence leads to the conclusion that a diffusion controlled process, such as boundary sliding, is dominant in the stress and temperature regimes considered in this work. Dislocation dynamics within α_2 plates would not be rate-controlling.

References

1. R.S. Mishra and D. Banerjee: "Microstructure and Steady State Creep in Ti-24Al-11Nb," to be published.

2. H.T. Kestner-Weykamp, C.H. Ward, T.F. Broderick and M.J. Kaufman: "Microstructures and Phase Relationships in the Ti_3Al + Nb System," *Scripta Metallurgica*, Vol. 23, (1989), pp. 1697-1702.

3. B. Walser and O.D. Sherby: "The Structure Dependence of Power Law Creep," *Scripta Metallurgica*, Vol. 16, (1982), pp. 213-219.

4. E.N.d.c. Andrade: "The Concept of Creep," in *Creep and Recovery*, Proceedings of the Thirty-Eighth Nat'l Metal Congress and Exhibition, Ohio, (1957), pp. 176-198.

5. S. Takeuchi and A.S. Argon: "Review: Steady-State Creep of Single-Phase Crystalline Material at High Temperature," *J. Mat. Sci.*, Vol. 11, (1976), pp. 1542-1566.

6. A.M. Brown and M.F. Ashby: "On the Power-Law Creep Equation," *Scripta metall.*, Vol. 14, (1980), pp. 1297-1302.

7. H.J. Frost and M.F. Ashby: *Deformation Mechanism Maps: The Plasticity and Creep of Metals and Ceramics*, Pergamon Press, Oxford, England, 1982, pp.11-14.

8. J. Weertman: "Dislocation Climb Theory of Steady-State Creep," *Trans. ASM*, Vol. 61, (1968), pp. 681-694.

9. F.R.N. Nabarro: "Deformation of Crystals by the Motion of Single Ions," in *Proceedings of the Bristol Conference on Strength of Solids*, London, (1948), Physical Society, pp. 75.

10. C. Herring: "Diffusional Viscosity of a Polycrystalline Solid," *J. Appl. Phys.*, Vol. 21, (1950), pp. 437-445.

11. H. Lüthy, R.A. White and O.D. Sherby, "Grain Boundary Sliding and Deformation Mechanism Maps," *Mater. Sci. Eng.*, Vol 39, (1979), pp. 211-216.

12. M.Mendiratta and H.A. Lipsitt: " Steady-State Creep Behavior of Ti_3Al-Base Intermetallics," *J. Mat. Sci.*, Vol. 15, (1980), pp. 2985-2990.

13. W. Cho, A.W. Thompson, and J.C. Williams: "Creep Behavior of Ti-25Al-10Nb-3V-1Mo," *Metall. Trans. A*, Vol. 21, (1990), pp. 641-651.

14. A.K. Mukherjee, J.E. Bird and J.E. Dorn: "Experimental Correlatiuons for High-Temperature Creep," *Trans. ASM*, Vol. 62, (1969), pp.155-179.

15. G. Malakondaiah and P. Rama Rao: "Creep of Alpha-Titanium at Low Stresses," *Acta Metall.*, Vol. 29, pp. 1263-1275.

16. D. McLean and M.H. Farmer: "The Relation During Creep Between Grain-Boundary Sliding, Sub-Crystal Size, and Extension," *J.Inst. Met.*, Vol. 85, (1957), pp.41-50.

17. W. Cho, J.W. Jones, J.E. Allison and W.T. Donlon: "Creep Behavior of Ti-6242: The Effect of Microstructure and Silicon Content," in *Proceedings of the Sixth World Conference on Titanium*, Vol. 1, Cannes, France, (1988), P. Lacombe, R. Tricot, and G. Béranger, eds., Les Éditions de Physique, Les Ulis, France, pp. 187-192.

18. D. McLean: "Grain-Boundary Slip During Creep of Aluminum," *J.Inst. Met.*, Vol. 81, (1952-53), pp. 293-300.

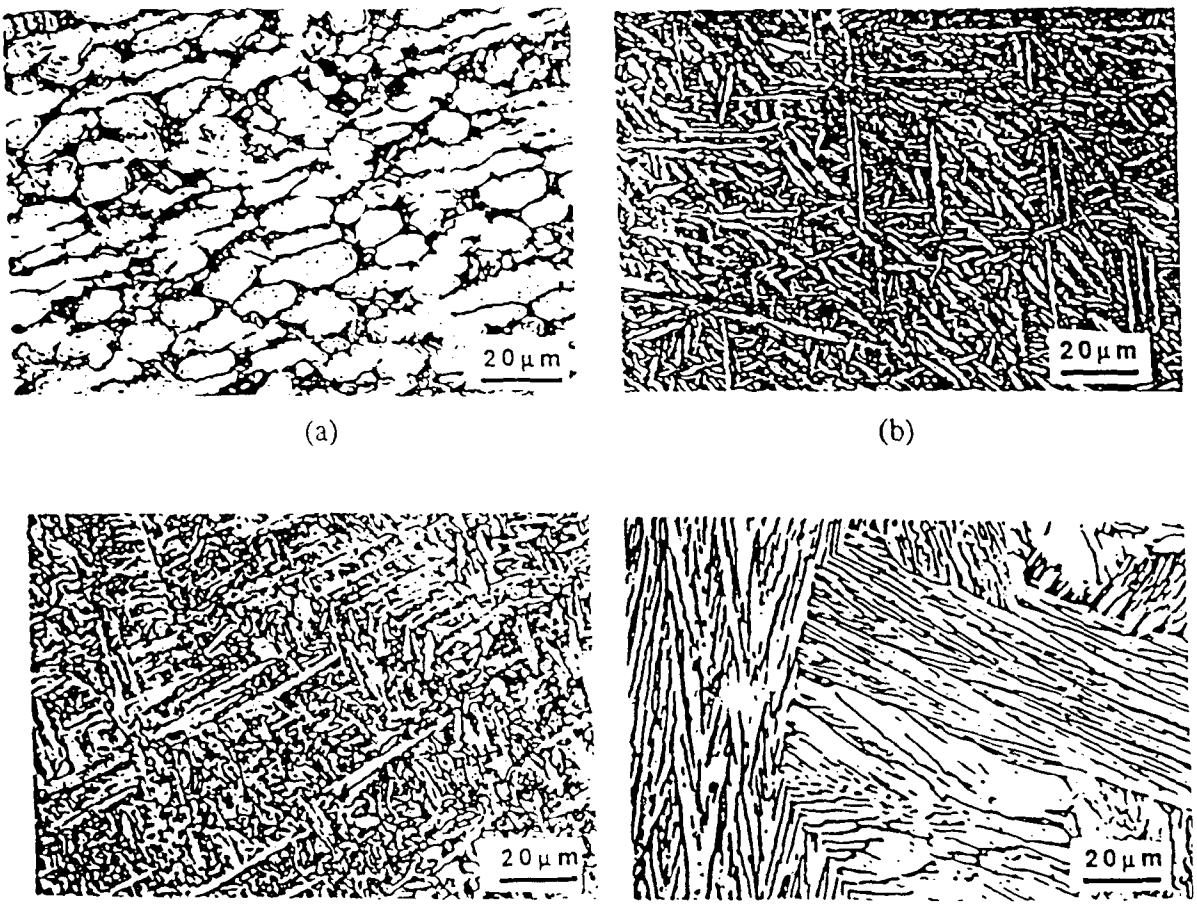

(a) (b)

(c) (d)

FIG. 1
(a) AR (b) 1200AC (c) 1000AC-15 (d) 1000AC-30.

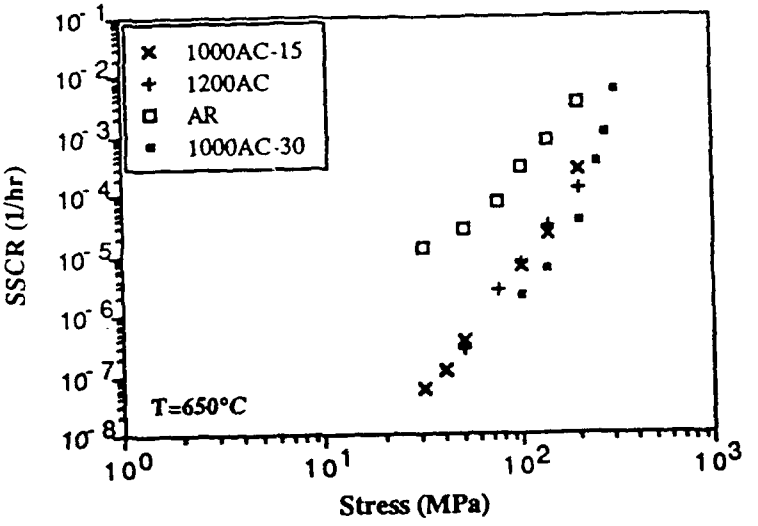

FIG. 2
SSCR *vs* σ for all microstructures at 650°C.

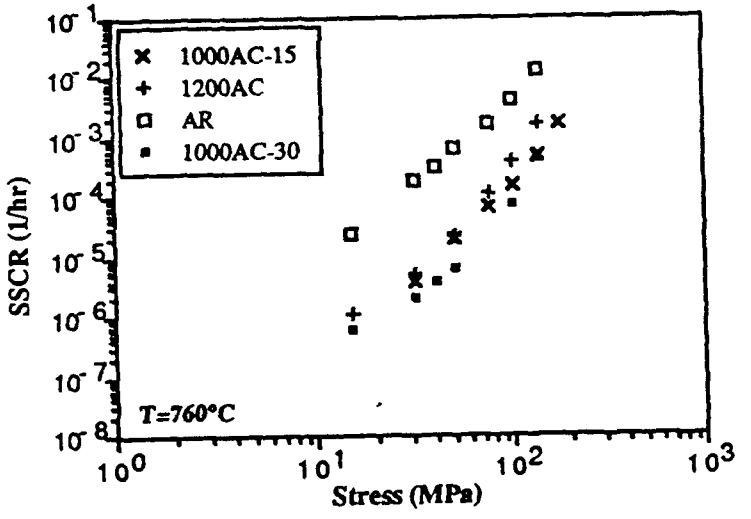

FIG. 3
SSCR *vs* σ for all microstructures at 760°C.

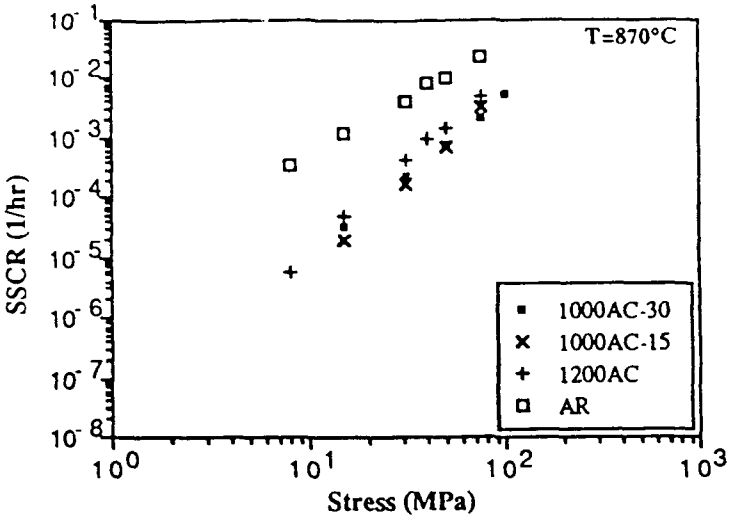

FIG. 4
SSCR *vs* σ for all microstructures at 870°C.

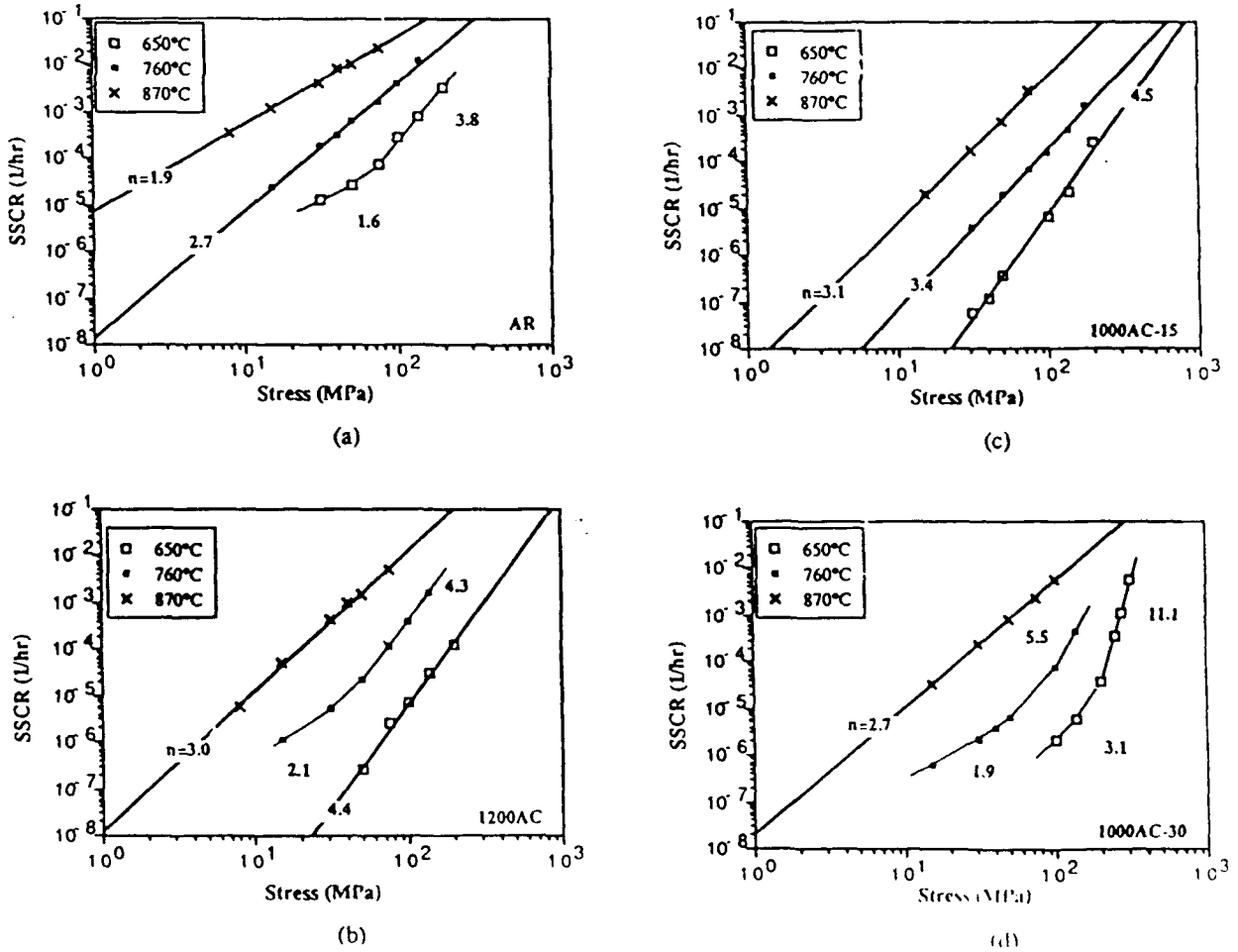

Figure 5 Effect of temperature on SSCR and n of (a) AR (b) 1200AC (c) 1000AC-15 (d) 1000AC-30

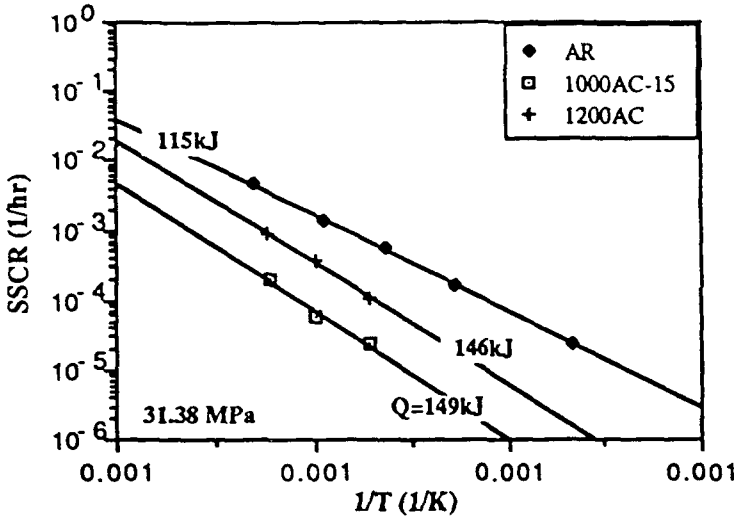

(a)

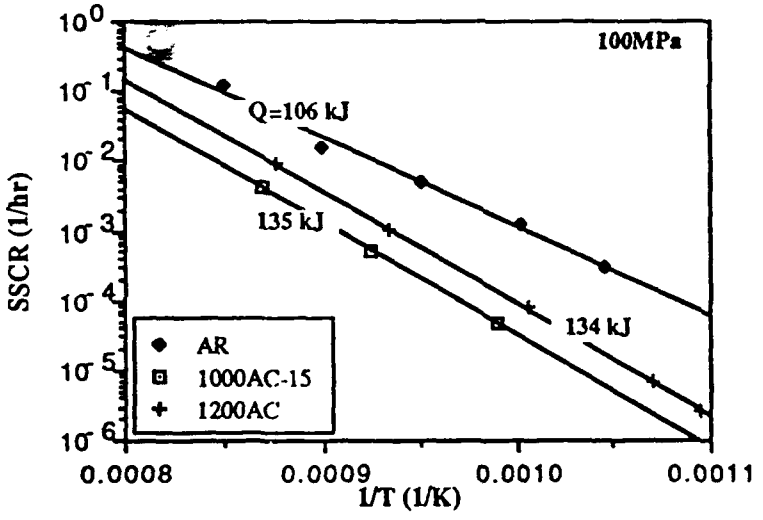

(b)

Figure 6. SSCR vs. 1/T at (a) 31.38 MPa (b) 100MPa

FUNDAMENTALS OF MECHANICAL BEHAVIOR IN ADVANCED INTERMETALLIC COMPOUNDS

J. M. Howe (Principal Investigator)
S. R. Singh (Research Associate)

Annual Report for 1st Year - Oct. 1, 1989 to Sept. 30, 1990

During the past year, our research has concentrated on determining the structure and deformation behavior of TiAl alloys containing the ternary additions Ta and Mn. These additions have been shown to improve the room-temperature ductility of TiAl and are possible candidate alloy systems for future high-temperature applications.

At the start of this program, we obtained four 18-lb., 4.5 inch diameter ingots with the following compositions (in atomic %) from Timet, Inc.: Ti-48Al, Ti-48Al-2Mn, Ti-52Al-2Mn and Ti-48Al-2Ta. The three alloys containing 48Al should consist of a γ-TiAl matrix with precipitates of the α_2-Ti_3Al phase, while the 52Al alloy should lie in the single-phase γ region of the phase diagram. These ingots were hot-extruded into 1 inch rod by the Materials Laboratory at Wright Patterson AFB. Pieces of the four rods were heat treated for microstructural examination by TEM. The remaining rods were then machined into tensile specimens for high-temperature deformation analysis.

So far, microstructural examination of the heat treated Ti-48Al and Ti-48Al-2Ta alloys has yielded several important results. One of the most interesting is that Ta has been found to lower the stacking-fault energy of TiAl and that this leads to extrinisic stacking-faults which serve as nuclei for twin lamellae (refer to attached Scripta Metall. et Mater. paper). Since twinning is an important deformation mechanism in these ordered alloys, such changes should significantly affect the room and elevated-temperature properties of TiAl, and this will be investigated shortly. The change in stacking-fault energy appears to be directly related to the electronic structure of Ta, and correlation among the electronic structure, deformation mechanisms and mechanical properties should allow us to understand these alloys on a fundamental level. This should be of great value in designing TiAl alloys with optimum mechanical properties. The addition of Ta to TiAl has also been found to alter the morphology and interfacial

structure of the α_2 phase in the TiAl matrix (refer to attached MRS Symp. Proc. paper). Although we do not yet know how the change in interfacial structure affects the deformation behavior, deformation of such two-phase alloys by both slip and twinning cannot occur without involving the interface and this is an important issue that will be investigated in coming months.

Several other projects either sponsored by AFOSR or directly related to the present grant were also performed during the past year (refer to attached Scripta Metall. et Mater. and Acta Metall. et Mater. papers). These include a high-resolution TEM analysis of the interphase boundary structure in a Ti-Cr alloy with Prof. H. I. Aaronson at CMU and the effect of coherency stress on the phase boundaries in Ti-Al alloys with Prof. W. C. Johnson, also at CMU. Both of these studies provide important fundamental information for understanding the formation and behavior of second phases in Ti-alloy matrices.

Research Plans for 2nd Year - Oct. 1, 1990 to Sept. 30, 1991

In the second year of this program we plan to concentrate on several areas of research. Firstly, we have begun microstructural analysis of the two Mn-containing TiAl alloys for comparison with the binary and Ta-containing alloy. The element Mn has also been reported to increase the room-temperature ductility of TiAl, possibly by changing the stacking-fault energy, and we intend to compare these alloys with the Ta-containing alloy where we observed such changes. We also plan to perform room and elevated-temperature tensile tests on the four alloys and to examine the deformed microstructures by TEM. The tensile specimens have been heat treated and machined and we are ready to begin these tests. *In situ* hot-stage straining in the TEM will also be performed on the most interesting alloys from the tensile results, to examine the specific mechanisms by which the alloys deform. This will provide a more complete understanding of the role of Ta and Mn on the deformation behavior of TiAl for correlation with the electronic structures of these elements. Hopefully, completion of these studies will establish a solid framework for understanding the role of alloying and microstructure on the deformation mechanisms in TiAl, which should be very useful in alloy design.

We have also begun to examine the microstructures of alloys containing higher Al, such as Ti_3Al_5 and $TiAl_3$. Small quantities of

these alloys were provided by Timet, Inc. The Ti_3Al_5 phase is not on the equilibrium phase diagram but is often found in rapidly solidified Ti-Al alloys and has been claimed to bound α_2 plates in TiAl-base alloys. Since very little is known about the Ti_3Al_5 phase, we have begun to establish the microstructure of this alloy. We then plan to begin investigating $TiAl_3$ and possibly $NbAl_3$ alloys near the end of this year.

Lastly, research that was begun on the structure and deformation mechanisms of the β/α_2 interface in a Ti-Al-Mo alloy by Mr. S. J. Rozeveld was postponed when Mr. Rozeveld decided to complete a study on measurement of residual stresses in composites by convergent-beam electron diffraction for his Ph.D. thesis. Mr. Rozeveld will resume work on the Ti-Al-Mo system after completing his Ph.D. in about March, 1991. We have acquired a hot-stage for the high-resolution TEM at CMU that should allow us to determine the mechanisms of growth of the β/α_2 interface. When this study is finished, it will provide definitive results concerning the structure and growth of the β/α_2 interface, which is important for understanding microstructural evolution and deformation in Ti_3Al-base alloys as well as from a fundamental viewpoint of b.c.c. → h.c.p. phase transformations.

Publications During 1st Year (attached)

S. R. Singh and J. M. Howe, "High-Resolution Electron Microscopy of Interfaces in TiAl Alloys", in Proc. XIIth International Congress for Electron Microscopy, San Francisco Press, CA, p. 316 (1990).

J. Y. Huh, J. M. Howe and W. C. Johnson, "Analytical Electron Microscopy of Coherent and Incoherent $\alpha + \alpha_2$ Phase Equilibria in a Ti-16.64 at% Al Alloy", Scripta Metall. et Mater., **24**, 2007 (1990).

S. R. Singh and J. M. Howe, "Effect of Ta on Twinning in TiAl", Scripta Metall. et Mater., in press.

S. R. Singh and J. M. Howe, "Effect of Ta on the Structure and Dynamics of γ/α_2 Interfaces in TiAl", Materials Research Society Symposium Proc., Vol. 213, in press.

T. Furuhara, J. M. Howe and H. I. Aaronson, "Interphase Boundary Structures of Intragranular Proeutectoid α Plates in a Hypoeutectoid Ti-Cr Alloy", Acta Metall. et Mater., submitted.

Presentations During 1st Year

S. R. Rozeveld and J. M. Howe. "Structure and Deformation of the β/α_2 Interface in a Ti-Mo-Al Alloy", TMS-AIME Fall Meeting, Indianapolis, IN, October, 1989.

J. M. Howe, "Phase Transformation Studies in Metallic Alloys by Atomic-Resolution Transmission Electron Microscopy", Dept. of Materials Science and Engineering, University of Pittsburgh, Pittsburgh, PA, November 2, 1989.

J. M. Howe, "Atomic-Resolution TEM of Phase Transformation Mechanisms in Metallic Alloys", National Institute for Standards and Technology, Gaithersburg, MD, November 15, 1989.

J. M. Howe and S. J. Rozeveld, "Effect of Crystal and Beam Tilt on Simulated High-Resolution TEM Images of Interfaces", XIIth International Congress for Electron Microscopy, Seattle WA, August, 1990.

S. R. Singh and J. M. Howe, "High-Resolution Electron Microscopy of Interfaces in TiAl Alloys", XIIth International Congress for Electron Microscopy, Seattle WA, August, 1990.

S. R. Singh and J. M. Howe, "Effect of Ternary Additions on the Structure and Dynamics of γ/α_2 Interfaces in TiAl", Materials Research Society Fall Meeting, Boston, MA, November, 1990.

in press

EFFECT OF Ta ON TWINNING IN TiAl

S. R. Singh and J. M. Howe
Department of Metallurgical Engineering & Materials Science
Carnegie Mellon University
Pittsburgh, PA 15213, U.S.A.

1. Introduction

TiAl alloy is a promising material for advanced aerospace applications because of its high strength, oxidation resistance and low density (1). However, its application is hindered by limited room-temperature ductility (2). Recent studies show that the ductility of TiAl can be improved by ternary element additions (3-7). The fundamental role of ternary additions in improving the ductility is still not clear, although deformation mechanisms pertaining to different types of dislocation activity have been proposed (2,8-11).

The TiAl alloy has an L1o structure, composed of layers of Ti and Al on alternate (002) planes, with a tetragonality of c/a=1.025 (Fig.1a). The Bravais lattice of the L1o structure is body-centered tetragonal with an axial ratio of $\sqrt{2}$:1, while the disordered structure is f.c.c. Twins in TiAl are of the $[11\bar{2}](111)$ type, which do not disturb the L1o symmetry of the lattice. Therefore, the TiAl lattice is often described as face-centered tetragonal.

Dislocation motion and twinning are the two principal modes of plastic deformation in TiAl (2,6,8-11). The high strength and low ductility of TiAl are attributed to complex superdislocation configurations. It is well known that materials which exhibit a low stacking-fault energy (SFE) deform by twinning. In connection with this, the ability of materials to show extensive faulting is determined by the ability of a perfect dislocation to dissociate into partials. Therefore, the SFE of a material determines whether deformation proceeds through the formation and propagation of partial or perfect dislocations. The effect of alloying additions on the SFE in TiAl is an important consideration for both the understanding and manipulation of mechanical behavior. Coherent twin boundaries have long been recognized as effective boundaries to plastic deformation in f.c.c. metals (12,13). Although twinning is thought to play an important role in deformation of ordered intermetallic alloys, the mechanisms by which this occurs have not received much investigation.

The present investigation describes the role of stacking faults and the effect of Ta additions on nucleation and growth of twins in TiAl. The role of these effects on the mechanical properties of the alloy is currently under investigation and will be discussed in a forthcoming paper.

2. Experimental Procedures

2.1 Alloy and Heat Treatment

The TiAl alloys in this study were produced by Timet as 8.2kg ingots 0.11m in diameter. The chemical compositions (at%) are shown below:

Alloy	Ti	Al	Ta	Fe	O	N
TiAl	51.20	48.45	0.00	0.049	0.289	0.008
TiAl-Ta	49.72	48.05	1.88	0.053	0.279	0.014

Pieces 2x4x1cm were cut from the ingots, wrapped in Ta foil, evacuated in quartz tubes to 10^{-3}Pa and then backfilled with Ar to 1/4atm pressure. The encapsulated alloys were heat treated in the single phase γ region at 1200°C for 2h and then in the $\alpha_2+\gamma$ phase field at 900°C for 24h, followed by water quenching.

2.2 Electron Microscopy

Thin-foil samples for transmission electron microscopy (TEM) were prepared by electropolishing in a 5% sulphuric-acid methanol solution at 20V and -40°C. When necessary, some of the thin foils were Ar ion-milled at an 8° angle in order to image a thicker area of interest by high-resolution transmission electron microscopy (HRTEM). After an initial investigation by conventional TEM was performed in a Philips EM 420T at 120kV, HRTEM was performed in a JEOL 4000EX operating at 400kV with an objective lens spherical aberration coefficient of Cs=1.1mm. The obtainable structural resolution is about 0.18nm. Images of twin interfaces were simulated using the TEMPAS multislice programs (14). Although a large supercell can be required to avoid spurious contrast due to periodic continuation (15) in image simulation, since the interfaces in TiAl are oriented end-on along the beam direction, the size of the supercell is determined purely by the extent of twin lamellae in the image plane rather than by the requirement of a large supercell imposed by periodic continuation.

3. Results and Discussion

3.1 Conventional TEM of Binary and Ternary Alloy

Figure 2(a) shows $[11\bar{2}](111)$ twins in the binary TiAl alloy. The overall microstructure consisted of twinned γ-TiAl and α_2-Ti_3Al with the following orientation relationship: $(111)_\gamma$ // $(0001)_{\alpha 2}$ and $[\bar{1}10]_\gamma$ // $[2\bar{1}\bar{1}0]_{\alpha 2}$. This is similar to the orientation relationship observed during the f.c.c.-->h.c.p. allotropic transformation in Co (16). The microstructure of the ternary TiAl alloy is shown in Fig. 2(b). The Ta addition did not change the overall microstructure but the twin thickness was reduced by a factor of about 4. Figures 3(a,b) are bright-field and dark-field images with the same operating reflection $g=\bar{1}11$, from a γ-TiAl area which was devoid of twins in the ternary alloy. This area contained a large number of faulted dipoles bounded by $a/6\langle 112 \rangle$ partial dislocations. In this image, the partial dislocation bordering the fault is invisible. A detailed contrast analysis showed that the faults are extrinsic in nature. These segmented faults were not observed in the binary alloy. The presence of these faults, the smaller twin width and additional cross twinning, all indicate that Ta lowers the SFE of the alloy. This possibility is further analyzed by HRTEM in the following section. It has been found that Mn-added TiAl shows unusual work hardening which is much higher than that of TiAl, thought to be caused by a decrease in SFE and/or stabilization of twin partial dislocations (4).

3.2 High-Resolution TEM of Binary and Ternary Alloy

The projected crystal structures of TiAl in $[\bar{1}10]$ and $[10\bar{1}]$ orientations are shown in Figs. 1(b) and (c), respectively. It can be seen that in a $[10\bar{1}]$ projection, the Ti and Al atoms are superimposed, whereas the $[\bar{1}10]$ projection shows that the Ti and Al atoms are alternately occupying the (002) planes. This leads to a (111) plane which is composed of columns of pure Ti and Al along $[\bar{1}10]$. A representative HRTEM image of coherent twins in a $[\bar{1}10]$ orientation in the ternary alloy is shown in Fig. 4. The twins are narrow and all the twin lamellae are in the same orientation. Figures 5(a-c) show two twin lamellae bounded by twin interfaces in a $[\bar{1}10]$ orientation and an isolated twin interface in a $[10\bar{1}]$ orientation, with the corresponding simulated image from the ternary and binary alloys, respectively. These images show that only the $\langle 110 \rangle$ oriented crystal reveals compositional information from the (002) planes. The ternary alloy had many more fine twins, such as the ones in Figs. 5(a,b), than the binary alloy.

Comparison between Figs. 5(a) and (c) shows that in a $[\bar{1}10]$ orientation, it is possible to obtain information about the composition of the (002) planes, because alternate (002) planes are composed of either Ti or Al atoms. In Fig. 5(a), the twinned region has a thickness of five (111) planes. Viewing along the (002) planes of either Ti or Al in the γ-TiAl matrix M and moving across the matrix-twin interface T1, one finds continuity of the Ti or Al planes in the matrix and twinned region, although in the twin lamella, the continuity is maintained along the (111) planes. By tracing the same lattice planes in a twinned region and moving across the twin-matrix interface T2, it was found that there is a compositional phase shift of one (002) plane, i.e., Ti planes crossing the interface T1 meet the Al planes at the interface T2. Figure 5(b) shows a HRTEM image of an eight-plane twin lamella. In this image, there is no compositional phase shift across the interfaces T1 and T2. It is concluded from these observations, that an odd number of (111) planes in a twin lead to a compositional phase shift across this defect, whereas an even number of (111) planes in the twin generates perfect compositional registry across the twin-matrix interface.

3.3 Analysis of Twin Lamellae

The presence or absence of compositional registry across a twin-matrix interface can also be derived by examining the passage of twinning partial dislocations a/6<11$\bar{2}$] in the matrix. The (111) planes consist of rows of Ti or Al atoms along [$\bar{1}$10] directions. In the L1o structure, the stacking of (111) planes can be approximated with a cubic close-packed stacking sequence of ABCABC... Since the distance between B and C sites measured parallel to the close-packed planes corresponds to a translation vector of a/6<11$\bar{2}$], passage of a single twinning partial in the matrix, whose Burgers vector is also a/6<11$\bar{2}$], leads to a relative shift of all the planes above the glide plane by a vector a/6<11$\bar{2}$], i.e., atoms above the glide plane are shifted from sites A, B and C to sites B, C and A, respectively. A compositional phase shift occurs across the twin interface when an odd number of partials is involved in twinning. A schematic representation in terms of the ABC... sequence is shown below.

```
A B C A|B C A B C|A B C A B C A B...
       C A B C A|B C A B C A B C...
         B C A B|C A B C A B C A...
           A B C|A B C A B C A B...
             C A|B C A B C A B C...
               B|C A B C A B C A...
-------------------------------------
A B C A|C B A C B|C A B C A B C A...
       h       h
```

Passage of a twinning partial in the matrix shifts the close packed positions to the right of the first vertical line in the top row from B-->C, C-->A and A-->B as shown in the second row. This shift from B-->C leads to a change in composition while a second shift restores the original composition in the third row. The vertical line and letter (h) indicate the interface plane and hexagonal orientation of the plane corresponding to the neighboring planes, respectively. In this representation of the five-plane twin the interface planes are A and B, which give a compositional phase shift. Similarly, the eight-plane twin has interface planes A and C, which are due to shifts from B-->C and C-->A. This even number of shifts does not produce a compositional phase shift. The twin lamella is bounded by two twin planes (h). In this representation, an intrinsic stacking-fault can be represented by two twin planes separated by one internal plane, whereas an extrinsic stacking-fault is represented by two twin planes separated by two planes. Therefore, the intrinsic stacking-fault should display a chemical shift of the (002) planes across the fault while an extrinsic-fault should not. The twinned region of the crystal may be thickened by producing either intrinsic stacking-faults on every close-packed plane or extrinsic stacking-faults on every other plane, leaving partial dislocations in the boundary. Energetically, if one disregards interactions beyond the fourth nearest-neighbor, then $\gamma_i = \gamma_e = 2\gamma_t$, where γ_i, γ_e and γ_t are the intrinsic, extrinsic and twin-fault energies respectively (18). This is because a stacking fault has two interfaces whereas a twin fault has only one.

The observed shear angle of the ($\bar{1}$11) plane across the twins in Fig. 5 was 39°, which gives rise to a shear strain of 0.708. This value is very close to the theoretical shear angle of 38.9° and shear strain of 0.707(=1/$\sqrt{2}$) for a f.c.c. crystal. This indicates that approximating the L1o structure to a f.c.c. structure is reasonable. Figure 6(a) shows an image of an extrinsic stacking-fault near the edge of a foil in the Ta-containing alloy. Figure 6(b) shows the intersection of an extrinsic stacking-fault (SF) and a three-plane twin on the (111) and ($\bar{1}$11) planes respectively. Many similar observations of extrinsic stacking-faults bounded by partials were made. For dissociated dislocations in the (111) slip plane and assuming isotropic elasticity, the relation between stacking-fault width and stacking-fault energy is given by (17). Using the elastic constants of TiAl (2) with $b^2 = 0.0266nm^2$ and our observed stacking-fault width of about 11-7.5nm yields a stacking-fault energy of γ_e = 18-27 mJ/m^2. Following the criterion of Hirth and Lothe (18) mentioned above for estimating the twin fault energy then gives γ_t = 9-13.5 mJ/m^2. For comparison, these experimentally determined values of the twin and stacking-fault energies (in mJ/m^2) with other available experimental and theoretical values are listed below.

Alloy	Temp. (K)	Intrinsic	Extrinsic	Twin	Remarks
TiAl	0	90	80	60	Theory (19)
TiAl	0	60			Theory (20)
$Ti_{46}Al_{54}$	293	70-85			Experiment (9)
$Ti_{46}Al_{54}$	873	60			Experiment (9)
$Ti_{50}Al_{48}Ta_2$	293		18-27	9-13.5	Expt. (Present)

The SFE of the TiAl-Ta alloy is much lower than the SFE values evaluated by others. Theoretical calculations (21) have shown that both intraplanar (001) Ti-d/Ti-d and interplanar (100) Ti-d/Al-p hybrid bonds are important to cohesion in stoichiometric TiAl. Further, it has been proposed (22) that the brittleness of the stoichiometric material could be attributed to large activation barrier to shear deformation as a result of a strong, directional p-d component of the bonding. It was suggested that strengthening of the intraplanar bonding and/or weakening of the interplanar p-d bonds would offer a plausible means of increasing the ductility of TiAl. One way of enhancing the d-d interaction is through substitution of an early transition metal for Ti. Theoretically this has been suggested to be more effective for substitutions from the 4d series than the 3d series. Perhaps this can be related to

the larger atomic volumes and more diffuse d-orbitals for the larger n-transition series. Given these observations it seems plausible that similar substitutions from 5d series (notably Ta) should have similar influence on the activation energy barrier to shear and consequently the SFE. This may be one possible reason for the low SFE reported above.

The observation of coexisting stacking faults and thin twins in the Ta-containing alloy indicates that the stacking faults act as nuclei for twin formation. These faults were formed by the expansion of dislocation loops. Since no deformation was applied to the specimens and both specimens were processed together, the observed stacking faults are thought to be introduced by thermal stresses during quenching. The preponderance of faults in the Ta-containing alloy as compared to the binary alloy indicates that Ta lowers the stacking-fault energy of TiAl. The growth of twin lamellae can be described as an initial development of a stacking-fault followed by nucleation of microtwins by superposition of extended faults on alternate planes. Finally, this nucleus is extended by propagation of the twin boundary in the matrix. As evident from Fig. 6(b), a stacking-fault presents a strong obstacle to glide dislocations on a conjugate close-packed plane. Although a stacking-fault is often treated as infinitely thin, it actually consists of two coherent twin-boundaries which form a microtwin. Coherent twin boundaries are known to act as obstacles to dissociated dislocations since a Shockley partial cannot simply cross a mirror plane (23). This non-conservation of Burgers vector which occurs for the translation of slip and/or for deformation twins which pass from matrix through the twin and vice-versa may lead to microscopic incompatibility, resulting in the development of local stresses at twin intersections. This may be one reason why twin boundaries appear to favor additional shear deformation parallel to an existing boundary rather than initiating a new twin on a conjugate slip plane.

4. Conclusions

This study employed HRTEM to identify thin twin lamellae and stacking-faults in TiAl by compositional phase shifts of (002) planes. The results and analyses presented show that extrinsic stacking-faults act as sites for twin nucleation. Subsequent thickening of twin lamellae is either due to superposition of extended stacking-faults on alternate close-packed planes or to passage of Shockley partials on every close-packed plane. Furthermore, addition of Ta to TiAl alloy appears to lower the SFE, which was estimated as 18-27 mJ/m^2 from the width of extended dislocations in HRTEM images of an alloy containing 1.88 at% Ta.

Acknowledgement

This work was supported by the Air Force Office of Scientific Research under Grant No. 90-0033. The authors are grateful to Prof. M. E. McHenry for helpful discussions on the electronic structure of TiAl.

References

1. J. B. MacAndrew and H. D. Kessler, J. Metals 8, 1348 (1956).
2. H. A. Lipsitt, D. Shechtman and R. E. Schafrik, Met. Trans. 6A, 1991 (1975).
3. M. J. Blackburn and M. P. Smith, U. S. Patent No. 4, 294, 615 (1981).
4. T. Hanamura, R. Uemori and M. Tamino, J. Mater. Res. 3, 656 (1988).
5. K. Hashimoto, H. Doi, K. Kasahara, T. Tsujimoto and T. Suzuki, J. Japan Inst. Metals, 52, 816 (1988).
6. E. L. Hall and S-C. Huang, MRS Symp. Proc. 133, 693 (1989).
7. T. Kawabata, T. Tamura and O. Izumi, MRS Symp. Proc. 133, 329 (1989).
8. D. Shechtman, M. J. Blackburn and H. A. Lipsitt, Met. Trans. 5, 1373 (1974).
9. G. Hug, A. Loiseau and P. Veyssiere, Phil. Mag. 57, 499 (1988).
10. V. K. Vasudevan, M. A. Stucke, S. A. Court and H. L. Fraser, Phil. Mag. Lett. 59, 299 (1989).
11. E. L. Hall and S-C. Huang, J. Mater. Res. 4, 595 (1989).
12. K. S. Raghavan, A. S. Sastri and M. J. Marcinkowski, Trans. AIME, 245, 1569 (1969).
13. S. Mahajan and G. Y. Chin, Acta Metall. 21, 173 (1973) and 22, 1113 (1974).
14. R. Kilaas, Proc. Ann. Meeting E. M. S. A. 45, 66 (1987).
15. P. M. Fields and J. M. Cowley, Acta Cryst. A34, 102 (1978).
16. J. W. Christian, Proc. Roy. Soc. A206, 51 (1951).
17. E. Aerts, P. Delavignette, R. Siems and S. Amelinckx, J. Appl. Phys., 33, 3078 (1962).
18. J. P. Hirth and J. Lothe, Theory of Dislocations, p. 294, McGraw Hill, New-York (1968).
19. C. L. Fu and M. H. Yoo, Phil. Mag. Lett. 62, 159 (1990).
20. M. Yamaguchi, Y. Umakoshi, T. Yamane, Dislocations in Solids, p. 77, University of Tokyo Press, Tokyo (1985).
21. M. Morinaga, J. Saito, N. Yukawa and H. Adachi, Acta Met. Mat. 38, 25 (1990).
22. M. E. Eberhart, R. M. Latanision and K. H. Johnson, Acta Met., 33, 1769 (1985).
23. R. Gleichmann, M. D. Vaudin and D. G. Ast, Phil. Mag. A51, 449 (1985).

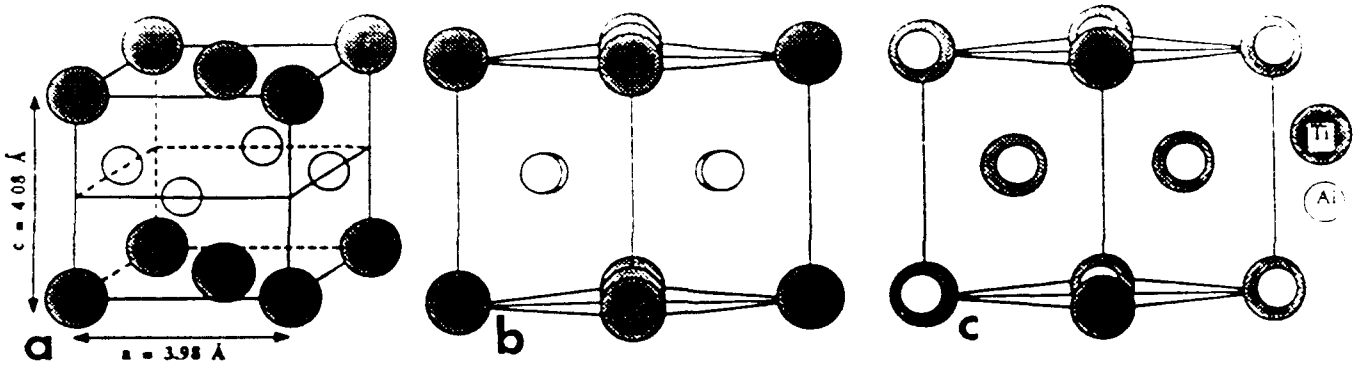

FIG. 1. (a) TiAl ($L1_0$) crystal structure with perspective views along (b) $[\bar{1}10]$ and (c) $[10\bar{1}]$.

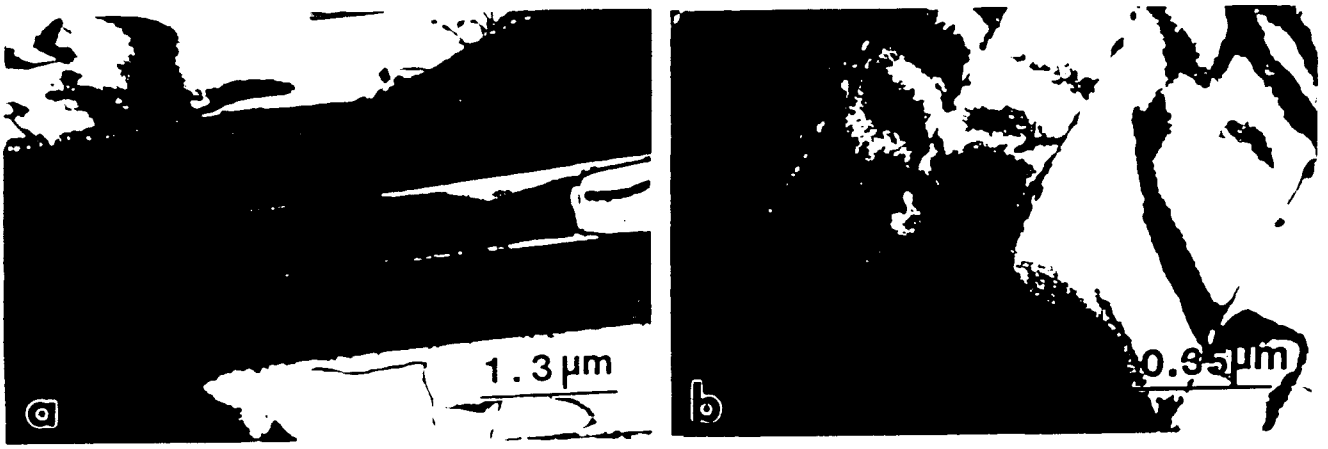

FIG. 2. Electron micrographs showing $[11\bar{2}](111)$ twins in (a) binary alloy and (b) ternary alloy.

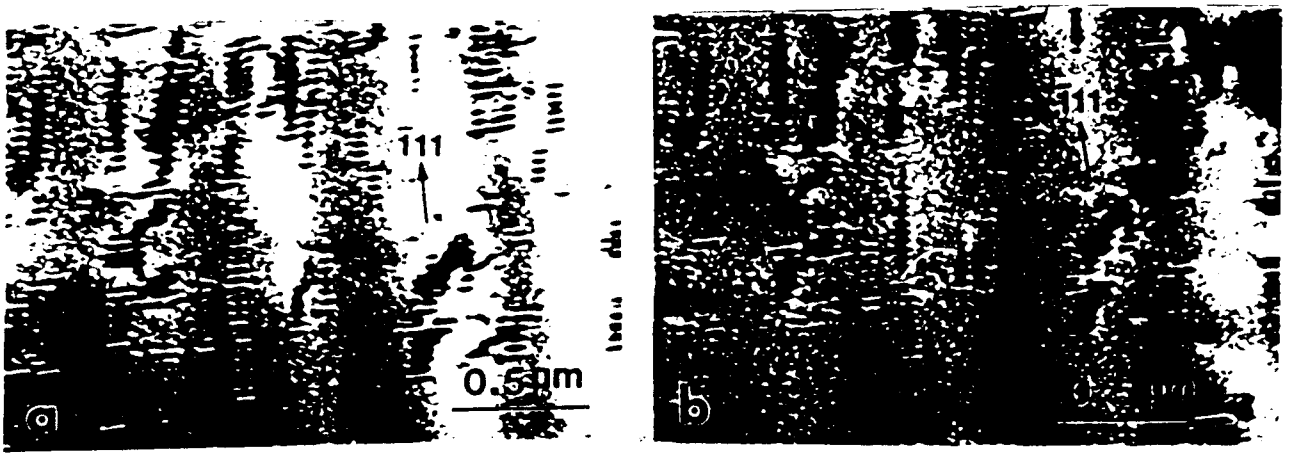

FIG. 3. Electron micrographs showing segmented stacking-faults in ternary alloy with operating reflection $g=\bar{1}11$ and $z=[211]$, (a) bright-field image and (b) dark-field image.

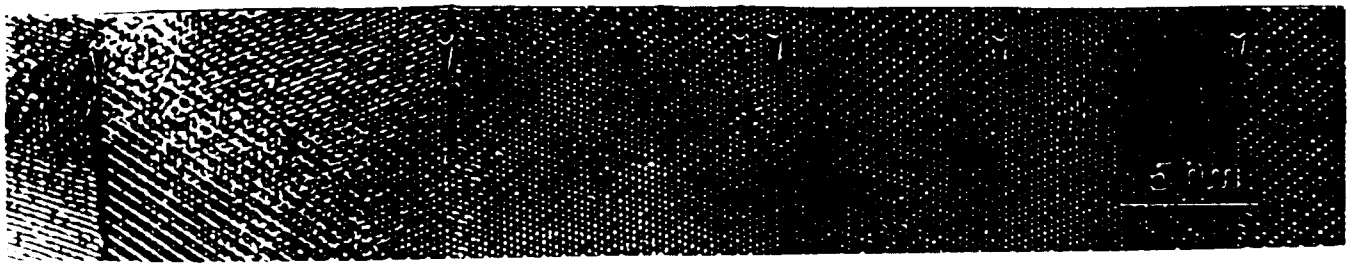

FIG. 4. HRTEM of twins in ternary alloy in $[\bar{1}10]$ orientation showing all the lamellae in the same orientation.

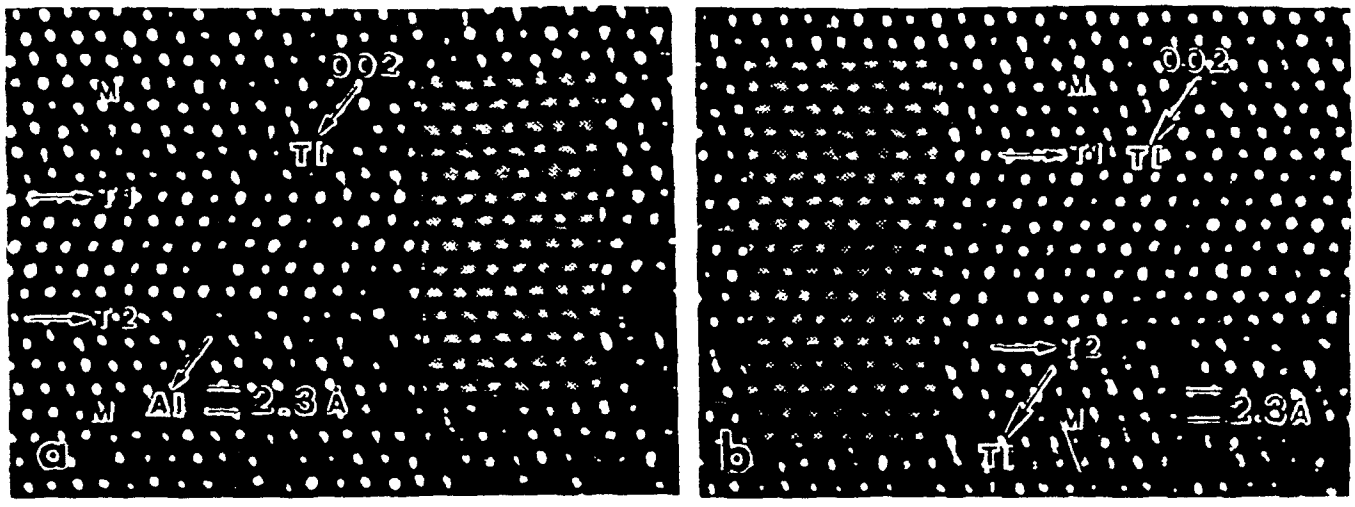

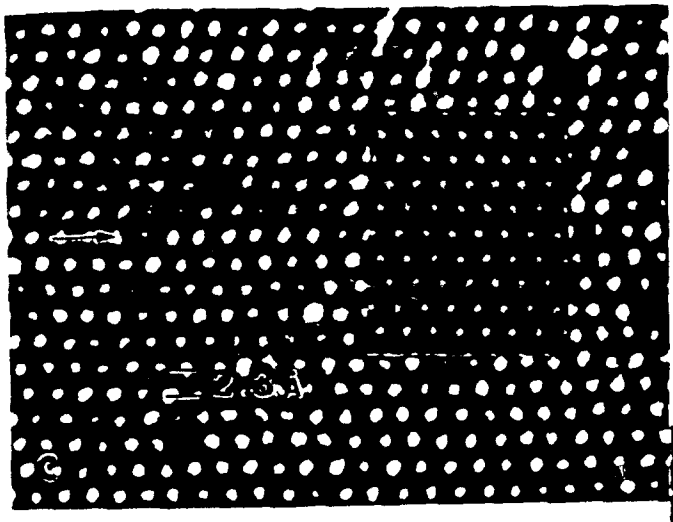

FIG. 5. HRTEM in [$\bar{1}$10] orientation of (a) five-plane thick twin lamella showing compositional phase shift of (002) planes in crossing the twin interfaces T1 and T2, (b) eight-plane twin lamella showing compositional registry of (002) planes across the twin interfaces T1 and T2, and (c) HRTEM of a twin interface in a [10$\bar{1}$] orientation.

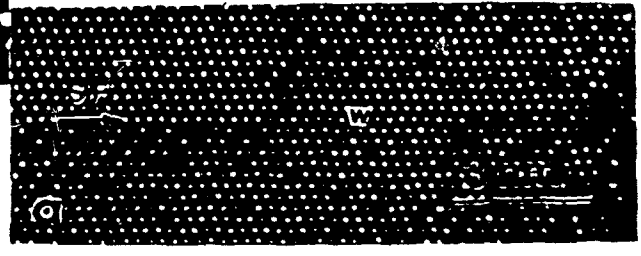

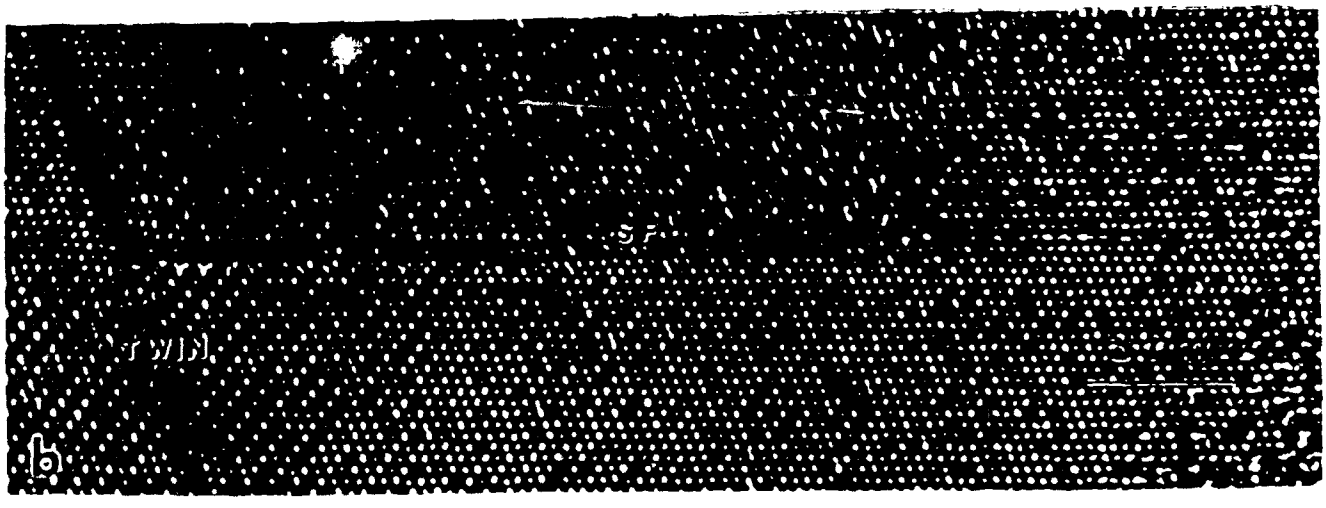

FIG. 6. HRTEM of ternary alloy showing (a) an extrinsic stacking-fault and (b) a stacking-fault twin interaction.

EFFECT OF Ta ON THE STRUCTURE AND DYNAMICS OF γ/α_2 INTERFACES IN TiAl

S. R. Singh and J. M. Howe
Department of Metallurgical Engineering & Materials Science, Carnegie Mellon University, Pittsburgh, PA 15213, U. S. A.

ABSTRACT

The structure of γ/α_2 interfaces in binary and Ta-containing TiAl alloys were analyzed by HRTEM and image simulations. Growth of α_2 was found to be due to a ledge mechanism, consisting of Shockley partial dislocations on alternate $(111)\gamma$ planes. The interface is atomically flat between the ledges and addition of Ta was found to transform arrays of growth ledges in the binary alloy into islands on the plate faces in the Ta-containing alloy. These islands of α_2 on the γ/α_2 interfaces were 4-7nm wide and increased in size with decreasing ageing temperature. The height of the ledges and islands were always a multiple of the c-parameter (0.46nm) of the α_2 phase. The islands were bounded by 90° (edge) and 30° (screw) Shockley partial dislocations. The 30° partial dislocation cores were localized whereas the 90° partial dislocation cores appeared to be highly delocalized due to presence of a high density of kinks, which in one case was found to be about $0.65nm^{-1}$.These results are interpreted in terms of the growth mechanisms and morphology of the α_2 phase.

INTRODUCTION

The intermetallic compound TiAl is an important structural candidate for use in high temperature applications. However its limited room temperature ductility has so far hindered its application [1-2]. It has been found that small amounts of ternary additions can improve the room temperature ductility of TiAl [3-7]. TiAl alloys can be classified into two categories, either single phase γ-TiAl or a two-phase mixture of γ-TiAl and α_2-Ti_3Al. The $\gamma+\alpha_2$ alloys are thought to have better mechanical properties than the single-phase γ alloys because the α_2 phase getters interstitial impurities [8], which improves the mechanical behavior. A recent study has shown that addition of Ta to TiAl reduces the stacking-fault energy and modifies the twinning behavior [9]. Therefore, this study was initiated to investigate the effect of Ta on the structure of the γ/α_2 interface in TiAl alloy. Development of TiAl with improved mechanical properties requires an understanding of the various interfaces in this alloy. Correlating the interfacial structure with ternary additions in TiaAl has important implications in alloy design. The γ/α_2 interface is discontinuous in chemical composition although structurally it is close to a simple f.c.c./h.c.p. interface. Explainingthe atomic-scale details of the γ/α_2 interface, particularly growth of unit-cell size islands, is a challenging problem even by high-resolution transmission electron microscopy (HRTEM).

γ-TiAl has a face-centered tetragonal $L1_0$ structure composed of alternate (002) planes of Ti and Al with a c/a ratio of 1.02, whereas α_2-Ti_3Al belongs to the h.c.p. structure-type DO_{19}. The γ and α_2 phases have the following orientation relationship (OR): $(111)\gamma//(0001)\alpha_2$ and $[-110]\gamma//[11\text{-}20]\alpha_2$, which is similar to the OR observed during the f.c.c.-->h.c.p. transformation in Co [10]. Many investigations into the interfacial structure and growth kinetics of precipitate plates in various diffusional transformations have been performed during last two decades [11, and references therein]. These investigations have provided important information about mechanisms of atomic attachment at the interface within the resolution limits of the techniques employed. In this regard, this study was undertaken to investigate the mechanism of growth of α_2 plates in TiAl and the effect of Ta on the interfacial structure of the γ/α_2 interface. The results from this HRTEM study show possible means of changing the interfacial structure.

EXPERIMENTAL PROCEDURES

The chemical compositions (at%) of the TiAl alloys investigated are shown below. Small pieces of alloy were wrapped in Ta foil and vacuum encapsulated in quartz tubes with a 1/4atm back pressure of Ar. The encapsulated alloys were solutionized at 1200°C for 2h and then isothermally aged for 24h in the $\alpha_2+\gamma$ phase field at 800°C, 900°C or 1000°C, followed by water

quenching. Thin-foil samples for transmission electron microscopy (TEM) were prepared by electropolishing in a 5% sulphuric-acid methanol solution at 20V and -40°C and Ar ion milling when necessary. Conventional TEM was performed in Philips EM 420T TEM at 120kV and HRTEM was performed in a JEOL 4000EX operating at 400kV with an objective lens spherical aberration coefficient of 1.1mm. In the TEM mode, ledges on the interfaces were identified by the displacement of extinction contours [12], whereas in HRTEM, direct observation of ledges on the faces and edges were made in <110>γ//<11-20>α2 orientations and kinks in the ledges were observed in a <111>γ//[0001]α2 orientation. Performing HRTEM in both orientations provided three-dimensional structural information about the interfaces. Images of interfaces were simulated using the TEMPAS multislice program [13]. In image simulation an appropriately large supercell was chosen to avoid spurious contrast due to periodic continuation [14].

Alloy	Ti	Al	Ta	Fe	O	N
TiAl	51.20	48.45	-	0.049	0.289	0.008
TiAl-Ta	49.72	48.05	1.88	0.053	0.279	0.014

RESULTS AND DISCUSSION

<110>γ//<11-20>α2 Oriented Interfaces in Binary TiAl

Fig. 1 shows a representative bright-field (BF) TEM image of dislocation ledges at the γ/α2 interface. Figs. 2(a) and 2(b) show HRTEM images of γ/α2 interfaces in the binary alloy in [-110] and [10-1] orientations, respectively. Since γ-TiAl has a tetragonal $L1_0$ structure, all the <110> directions are not equivalent, i.e., in a <110] projection alternate (002) planes consist of Ti or Al whereas in a <101] orientation, the Ti and Al atoms are superimposed because (100) or (010) planes are composed of both Ti and Al atoms. (The notation <hkl] indicates a fixed l with permutations of h and k.) In Fig. 2(a), contrast due to alternate (002) planes of Ti and Al when viewed along [110]γ is clearly visible. The γ/α2 interface indicated by an arrow is coherent and the interface plane is (111)γ//(0001)α2. Ledges that were two (111)γ planes high were visible in thicker parts of the crystal. Fig. 2(b) shows the γ/α2 interface viewed along the [101]γ direction. This interface is composed of coherent terraces parallel to (111)γ//(0001)α2 and an array of ledges (periodicity of 15nm) four (111)γ planes high. Two ledges separated by about 2-2.5nm are grouped together as if one is leading and the other is trailing. This arrangement of grouped ledges suggests that the velocity of the trailing ledge is faster than that of the leading ledge due to overlapping diffusion fields [15,16]. During the initial stage of plate growth, the ledges may be two planes high, while at later stage, two ledges may merge to form four-plane ledges. Slight displacement of the (111)γ and (0001)α2 planes normal to the Burgers vector of the ledge dislocations is evident, and this leads to **g·bxu** contrast [17], which can be seen as strain contrast in conventional BF images, as shown in Fig. 2(c) for an array with a periodicity of 15nm. Due to the presence of this regular array of ledges, the overall habit-plane of the γ/α2 interface differs from microscopic habit-plane mentioned above. The habit plane determined from the HRTEM image was found to be (443)γ, which makes an angle of 7.3° from (111)γ. The above observations clearly show that α2-plates in binary γ-TiAl thicken by movement of dislocation ledges along their faces on alternate {111}γ matrix planes, and that this accomplishes γ-->α2 transformation necessary for growth of α2 plates [18].

Fig. 1. Bright-field micrograph showing dislocation ledges (marked by arrows) at the γ/α2 interface in TiAl.

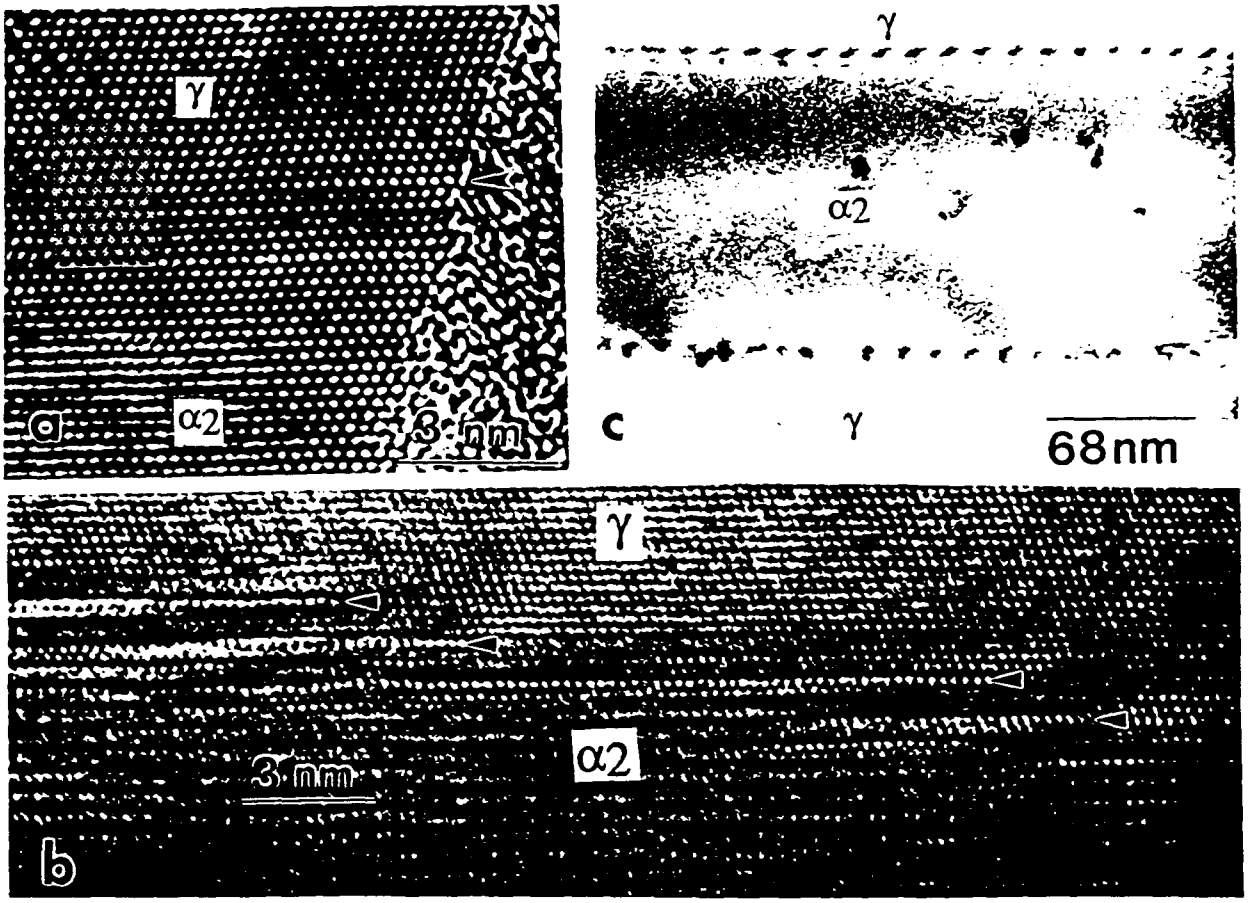

Fig. 2. <110>γ//<11-20>α2 HRTEM images of interfaces in binary TiAl: (a) [-110]γ orientation with simulated image as inset, (b) [10-1]γ orientation, and (c) bright-field TEM image corresponding to (b) showing strain contrast at the dislocation ledges.

<110>γ//<11-20>α2 Oriented Interfaces in Ta-Containing TiAl

It was mentioned in the Introduction, that addition of Ta to TiAl reduces the stacking-fault energy and modifies the deformation characteristics of the alloy. Figs. 3(a,b) show HRTEM images from the Ta-containing TiAl. Contrary to the array of ledges at the γ/α2 interface in binary TiAl, the interface in Fig. 3(a) consists of two-plane islands of α2 on an otherwise planar (111)γ//(0001)α2 interface. A glancing angle view along the (111)γ planes shows that they are parallel to (0001)α2, and that they are continuous as they cross the edges of the islands to become the (0001)α2 planes. This indicates that the edges of the ledges are coherent in this orientation. The islands were always found to be two atomic-planes high, i.e., the height of the unit-cell (c=0.462nm) along [0001]α2. The width of the islands parallel to the (0001)γ planes was about 5nm for the alloy aged at 900°C. The island widths for the alloy aged for the same time at 800°C and 1000°C were 7nm and 4nm, respectively. These limited data indicate that the island size increases with decreasing temperature, as might be expected since the driving force for growth increases with decreasing ageing temperature.

The island enclosed in Fig. 3(a) is bounded by 90° and 30° Shockley partial dislocation ledges, as indicated in Fig. 3(b). The Burgers vector of the 90° Shockley partial dislocation lies perpendicular to the [1-10] electron beam direction with a/6[-1-12], whereas for a 30° Shockley partial dislocation, the Burgers vector lies at an angle of 30° to the electron beam and is either a/6[2-1-1] or a/6[-12-1]. The Burgers circuits showing closure failure around these dislocations were drawn following the procedures described by Howe et al. [19]. Careful examination of the 30° partial dislocation core indicates that it is localized, whereas the core of the 90° partial dislocation appears highly delocalized. The diffuseness of the 90° partial dislocation core may be due to the presence of a high density of kinks along the ledge. These kinks act as attachment sites for atoms during the γ-->α2 transformation, where growth occurs by lateral migration of kinks

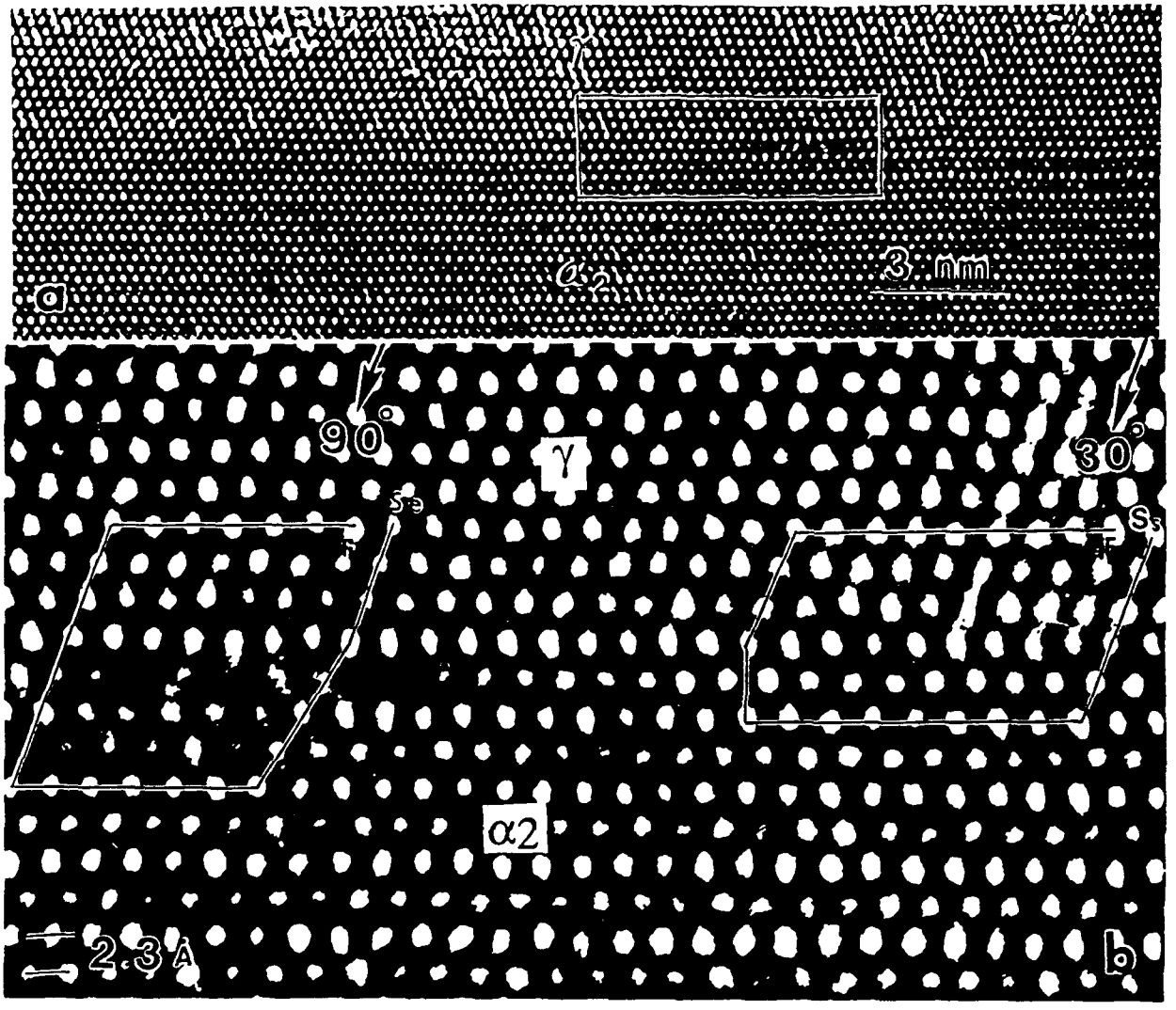

Fig. 3. <110>γ//<11-20>α2 HRTEM images of interfaces in Ta containing alloy showing: (a) islands of α2 on the faces, (b) enlargement of (a) with Burgers circuits around the 90° and 30° Shockley partial dislocations, and (c) γ/α2 interface at a plate edge with Burgers circuits (on next page). S_e, S_S and F are start of 90°(edge), 30°(screw) Shockley partial dislocations and finish points of Burgers circuits respectively.

in ledges parallel to the <110>γ direction and subsequent extension of the ledges along the <112>γ direction. This situation is analogous to that treated by Burton et al. [20] for crystal growth from a vapor or liquid and extension of these ideas to solid state transformation by Aaronson [21] and Howe et al. [19]. Therefore, the transformation site is at the kinks in the ledges, presumably with a point-source diffusion field around each kink. A direct view of these kinks can be obtained in a <111>γ//<0001>α2 orientation, as discussed in the next section.

The observations above were made only on the faces of the α2 plates. The edges and corners of the α2 plates also contain important information regarding the type and proportions of dislocations associated with the ledges during growth. A HRTEM image of a corner is shown in Fig. 3(c). The Burgers circuits drawn across the edge containing eight (0002)α2 planes shows a closure failure corresponding to three 30° Shockley partial dislocations and one 90° Shockley partial dislocation. Therefore, a total of four partial dislocations is associated with the growth of eight planes of α2 plates. This confirms that the α2 plates grow by the passage of Shockley partial dislocations on alternate (111)γ planes. The ratio of 30° to 90° partials was found to be 3:1 over a large segment of interface, which is in contrast to the ratio of 2:1 found in growth of γ (Ag_2Al) plates in the Al-Ag system [19]. A partial dislocations ratio of 2:1 indicates that all three type of dislocations involved in the transformation are in equal proportion and that no net shape-change occurs at the edge. Therefore, the observation of a partial dislocation ratio of 3:1 should introduce some kind of displacement or strain at the edges.

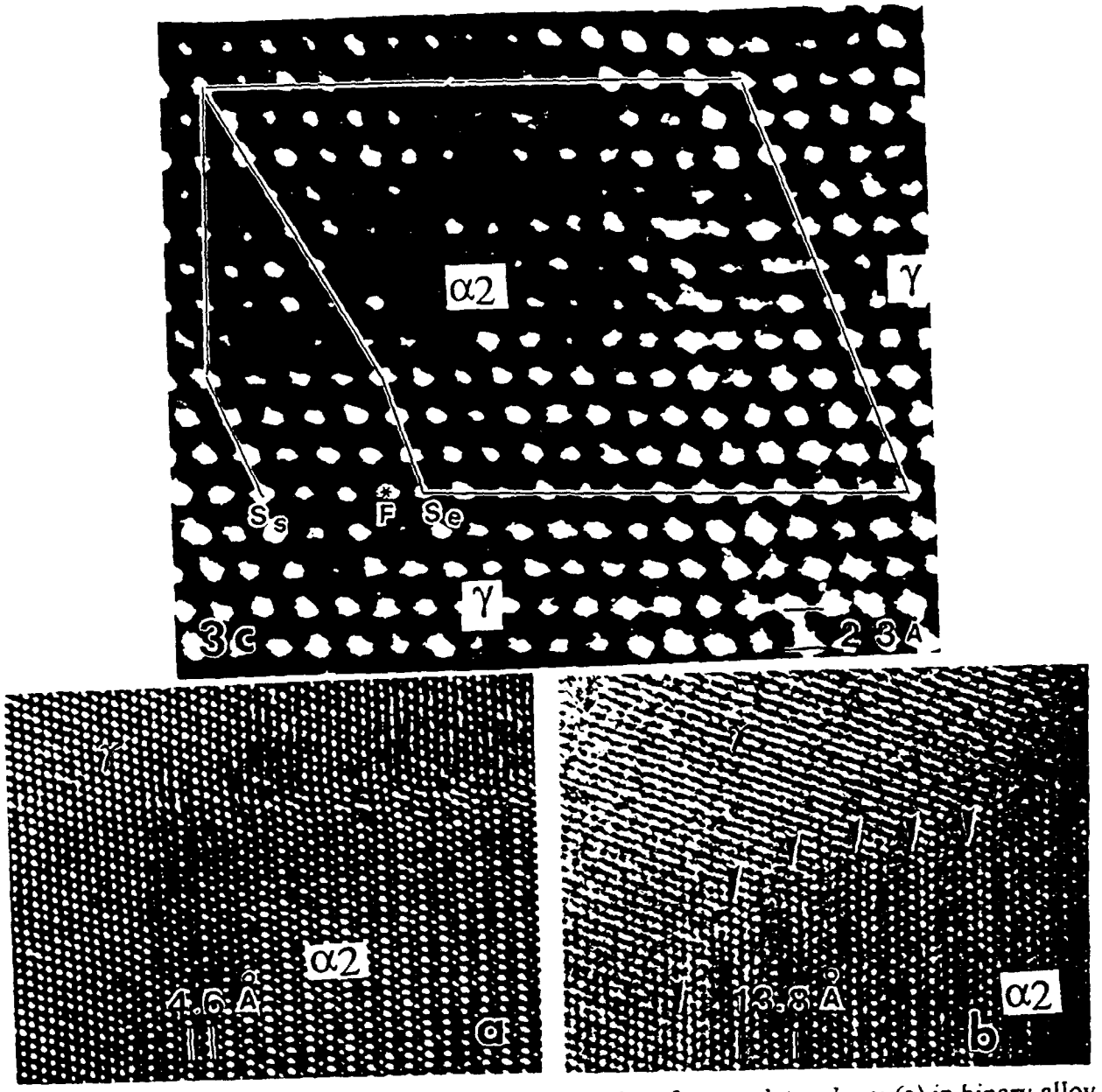

Fig. 4. <110>γ//<11-20>α2 HRTEM images of γ//α2 interface at plate edges: (a) in binary alloy showing distortion of (111)γ and (0001)α2 planes, and (b) in Ta alloy showing 6H-α2 stacking.

The growth of α2 plates due to passage of Shockley partials can be divided into three classes. (1) No net shape-change is observed when an equal number of all three Shockley partials accomplishes the transformation. This is favored because it minimizes the strain energy of the interface. (2) A net shape-change is observed when identically oriented Shockley partials on every other (111)γ plane are involved in the transformation and this maximizes the strain energy. (3) A partial shape-change or distortion is produced when unequal numbers of the three Shockley partials are involved. The present observations fall into class 3, in which the strain is accommodated in either of two ways: (1) by distortion in the planes at the edge of the plate, or (2) by additional slip which changes the normal ABAB... stacking sequence of the α2 plate. Both types of strain accommodation were observed in this investigation, as described below.

Figs. 4(a,b) are HRTEM images of the edges of α2 plates in the binary and ternary alloys, respectively. Fig. 4(a), obtained from the binary alloy, shows distortion of the (111)γ and (0001)α2 planes near the interface, whereas Fig. 4(b) from the ternary alloy shows a six-plane periodicity at the edge of the α2 plate. If this six-plane periodicity were an actual structure, then it could act as a transition phase between equilibrium γ and α2. Three possible alternatives to an equilibrium α2 structure were postulated in order to identify the six-plane structure: (1) a six-plane α2 Ti_3Al structure called 6H-α2, having a stacking sequence of ABCACB... instead of the

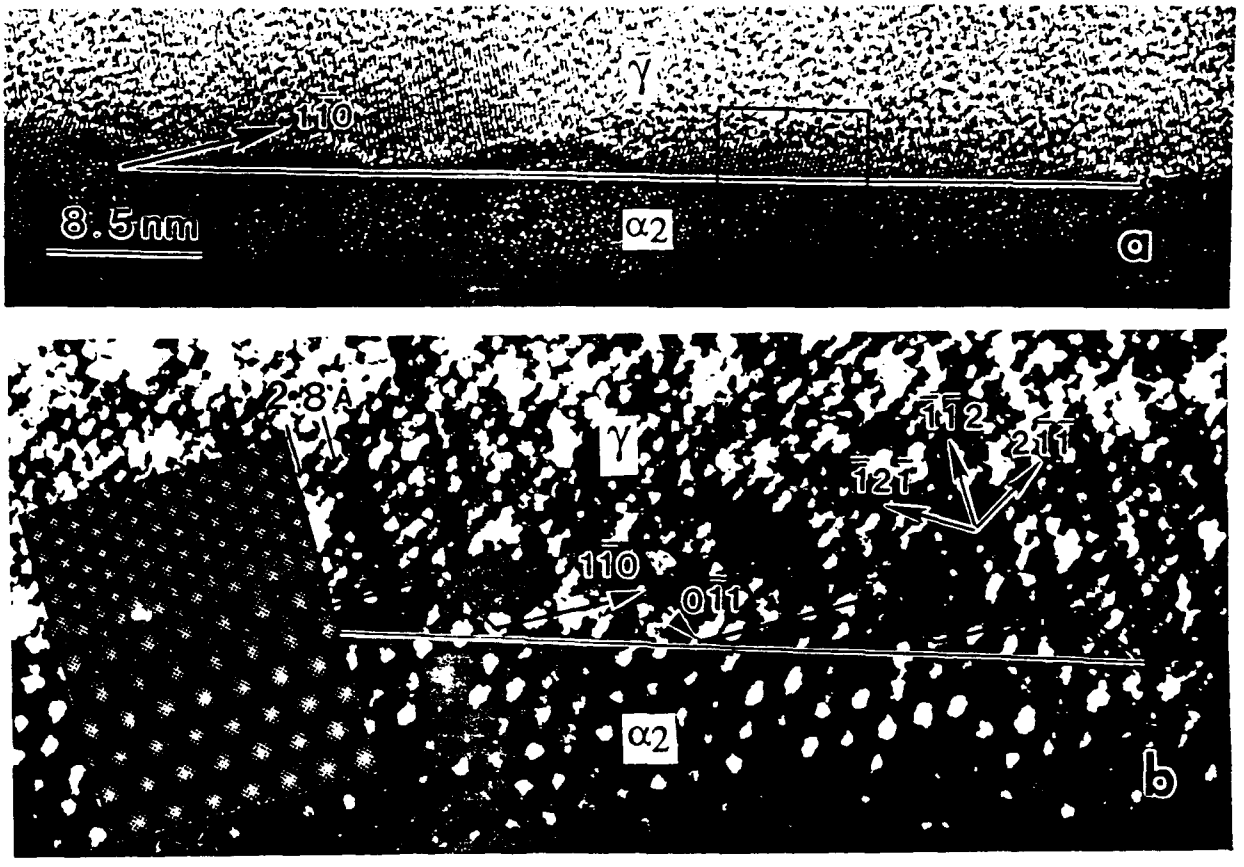

Fig. 5. [111]γ//[0001]α2 HRTEM images of γ/α2 interface in Ta alloy: (a) showing deviation of interface direction, and (b) enlargement showing faceting of interface due to kinks, and simulated image as inset.

usual ABAB... sequence of α2 and the same space group as that of α2, i. e., P63/mmc, (2) the transition phase Ti_2AlN [22], which has the same c-parameter as that of 6H-α2 and may form due to accummulation of N at the edges, and (3) a six-plane periodicity produced by a Moire effect due to superimposition of the α2 and γ phases at the edge in the HRTEM images. Image simulations of these three possible structures were performed. The second and third possibilities were eliminated due to poor and inconsistent image matching, respectively. The 6H-α2 gave a good match with the experimental images. Therefore, in the ternary alloy, a six-layer structure appears to be produced at the edges due to extra periodic slip from an unequal number of the three type of Shockley partial dislocations, instead of the normal two-layer structure of α2 in the binary alloy. Conversely, in the binary alloy, production of similar partial dislocations for the transformation leads to local distortion of the (111)γ and (0001)α2 planes near the edge.

The difference in results for the <110>γ//<11-20>α2 interfacial structures on the faces of the binary and Ta alloys can be explained as due to equilibrium and kinetic effects, respectively. These differences in interfacial structure and growth also give rise to thicker α2 plates in the binary alloy than in the ternary alloy, and this was verified by measuring the aspect ratios in electron micrographs.

<111>γ//<0001>α2 Oriented Interfaces in Ta-Containing TiAl

A low-magnification image of the <111>γ//<0001>α2 interface is shown in Fig. 5(a). Ledges on the edges of the α2 plates have a corrugated appearance with a spacing of about 11nm. An enlarged view of the enclosed area near the center of Fig. 5(a) is shown in Fig. 5(b). In this orientation, the coherency of the {220}γ//{11-20}α2 planes is evident from their continuity across the interface. Due to the ordered structure of the γ phase, alterna. (2-20) planes are occupied by either Ti or Al atoms, whereas this is not the case for the (0-22) and (-

202) planes. In Fig. 5(b), the interface is composed of relatively large kinks in the [1-10] direction and shorter kinks in the [0-11] direction. This gives rise to an interface direction close to [2-31], which deviates about 17.3° from the [1-10] direction. Following the relationship between kink concentration and the deviation of the average dislocation line direction from the direction of the Peierls valley [23], the calculated kink density was 0.63nm^{-1}. This value is in reasonable agreement with a kink density of 0.65nm^{-1}, which was measured from the HRTEM image shown in Fig. 5(b). The kinks at the interface are two atomic planes high or one γ unit-cell high. This indicates that the basic building block is two (110)γ planes high. This requirement is imposed by the ordered structure of alternate rows of Ti and Al atoms in the close-packed planes of the γ phase rather than by kinetics. This also shows that the α_2 phase grows by the lateral migration of kinks in the ledges parallel to the <110>γ directions rather than by overall movement of the <110>γ//<11-20>α_2 interface normal to itself, similar to the case of Shockley partial dislocation ledges in Al-Ag [19], although the ordered arrangements in γ and α_2 appear to impose additional requirements on the kinks in TiAl alloys.

CONCLUSIONS

The above analyses demonstrated that addition of Ta to TiAl greatly modifies the interfacial structure and morphology of the α_2 plates under the conditions of constant ageing time and temperature. The important findings are summarized as follows: (1) α_2 plates in TiAl alloys grow by passage of Shockley partial dislocations on alternate {111}γ planes where the 90° partial dislocation core appears to be less localized than the 30° partial core, (2) α_2 plates in binary TiAl grow by a regular array of ledges which changes the overall habit-plane, while isolated islands are predominant in the Ta-containing alloy, implying that Ta increases the ease of two-dimensional nucleation of ledges, (3) the γ/α_2 interfaces are coherent and faceted along low-energy <110>γ//<11-20>α_2 and <111>γ//[0001]α_2 directions at the unit-cell level, although arrays of ledges and facets can change the overal habit-plane and interface direction, (4) the width of islands on the faces of α_2 decreases with increasing ageing temperature due to a reduction in the driving force for island growth with increasing temperature, and (5) transformation strains may be accommodated by a possible 6H transition structure at the edges of an α_2 plate.

ACKNOWLEDGEMENTS

This work was supported by the Air Force Office of Scientific Research under the Grant No. 90-0033.

REFERENCES

[1] J. B. MacAndrew and H. D. Kessler, J. Metals 8, 1348 (1956).
[2] H. A. Lipsitt, D. Shechtman and R. E. Schafrik, Met. Trans. 6A, 1991 (1975).
[3] M. J. Blackburn and M. P. Smith, U. S. Patent No. 4, 294, 615 (1981).
[4] T. Hanamura, R. Uemori and M. Tamino, J. Mater. Res. 3, 656 (1988).
[5] K. Hashimoto, H. Doi, K. Kasahara, T. Tsujimoto and T. Suzuki, J. Japan Inst. Metals, 52, 816 (1988).
[6] E. L. Hall and S-C. Huang, MRS Symp. Proc. 133, 693 (1989).
[7] T. Kawabata, T. Tamura and O. Izumi, MRS Symp. Proc. 133, 329 (1989).
[8] V. K. Vasudevan, S. A. Court, P. Kurath and H. L. Fraser, Scripta Met. 23, 907 (1989).
[9] S. R. Singh and J. M. Howe, Scripta Met. Mater., submitted (1990).
[10] J. W. Christian, Proc. R. Soc. A206, 51 (1951).
[11] H. I. Aaronson, T. Furuhara, J. M. Rigsbee, W. T. Reynolds, Jr. and J. M. Howe, Met. Trans. 21A, 2369 (1990).
[12] H. Gleiter, Acta Met. 17, 565 (1969).
[13] R. Kilaas, Proc. Ann. Meeting E.M.S.A. 45, 66 (1987).
[14] P. M. Field and J. M. Cowley, Acta Cryst. A34, 102 (1978).
[15] G. J. Jones and R. Trivedi, J. Cryst. Growth 29, 155 (1975).

[16] C. Atkinson, Proc. Roy. Soc. A384, 167 (1982).
[17] P. B. Hirsch, A. Howie, R. B. Nicholson, D. W. Pashley and M. J. Whelan, Electron Microscopy of Thin Crystals, (Butterworth, Washington, 1965), p. 258.
[18] G. J. Mahon and J. M. Howe, Met. Trans. 21A, 1655 (1990).
[19] J. M. Howe, U. Dahmen and R. Gronsky, Phil. Mag. A 56, 31 (1987).
[20] W. K. Burton, N. Cabrera and F. C. Frank, Phil. Trans. Roy. Soc. 243, 299 (1951).
[21] H. I. Aaronson, Decomposition of Austenite by Diffusional Processes, (Interscience, New York, 1962), p. 387.
[22] M. J. Kaufman, D. G. Konitzer, R. D. Shull and H. L. Fraser, Scripta Met. 20, 103 (1986).
[23] J. P. Hirth and J. Lothe, Theory of Dislocations, 2nd Ed. (John Wiley & Sons, New York, 1982), p. 173, 490-492, 532-546.

Proceedings of the XIIth International Congress for Electron Microscopy

HIGH-RESOLUTION ELECTRON MICROSCOPY OF INTERFACES IN TiAl ALLOYS

S. R. Singh and J. M. Howe

Department of Metallurgical Engineering and Materials Science,
Carnegie-Mellon University, Pittsburgh, PA 15213, U.S.A.

Alloys based on TiAl are being considered as potential candidate materials for advanced aerospace applications. The interphase interfaces and twin interfaces in these alloys play important roles during deformation and can vary with ternary additions. Various HREM studies of interphase interfaces have been made in metallic systems during the last few years.[1,2] When combined with image simulations, HREM has the capability of revealing local structural and compositional information.[3,4] This investigation discusses HREM analyses of the crystallography of $\gamma/\alpha 2$ interfaces, twin interfaces and stacking faults in γ-TiAl with ternary additions of Mn and Ta.

The γ-TiAl alloys were solutionized at 1200°C for 2 hrs, isothermally aged for 24 hrs at 900°C in the $\alpha 2+\gamma$ phase field and quenched. Thin foil specimens were polished in a 5% sulphuric acid/methanol electrolyte at -40°C and 20V. The samples were examined in Philips EM420T and JEOL 4000EX microscopes at 120 and 400 kV, respectively. Image simulations were perfomed with the TEMPAS multislice programs,[5] using typical operating conditions for a JEOL 400EX.

Since the γ-TiAl phase has an $L1_0$ structure, the <110> directions are not all equivalent. Slip in the <110] direction does not disturb the ordered structure making it a favourable slip system, whereas <101] slip can destroy the ordered structure and result in a series of complex faults.[6] This slip system is feasible only if the dislocations move in pairs. With this background, the structures of $\gamma/\alpha 2$ interfaces in <110] and <101] orientations were investigated by HREM and the corresponding HREM images are shown in Figs. 1 and 2. In the <110] image in Fig. 1, the γ phase displays contrast characteristic of alternating (002) planes of Ti and Al. These planes extend to the interface, which is atomically flat and perfectly coherent between ledges that are two $(111)_\gamma$ planes high. In the <101] orientation in Fig. 2, the interface is also atomically flat but groups of two ledges, each of which is four $(111)_\gamma$ planes high, repeat periodically with a spacing of about 14 nm. Although the orientation relationship in both cases is $[110]_\gamma // [11\bar{2}0]_{\alpha 2}$ and $(111)_\gamma // (0001)_{\alpha 2}$, Fig. 2 also reveals that the average or microscopic habit plane is not $(111)_\gamma$ but $(443)_\gamma$, which makes an angle of about 7° from $(111)_\gamma$.

Figures 3 and 4 show experimental and simulated HREM images, respectively, of a twin that is five $(111)_\gamma$ planes thick in a <110] orientation. The twinning shear strain measured from the image is 0.7, which is close to the theoretical shear strain of 0.707 for a f.c.c. structure. These figures also show a compositional phase shift across the twin, i.e., the $(002)_\gamma$ Ti planes in matrix M1 connect to mixed $(111)_\gamma$ Ti+Al planes in twin T, which in turn connect to $(002)_\gamma$ Al planes in matrix M2. Since twinning of each $(111)_\gamma$ plane causes a displacement of a/6<112>, such a compositional phase shift will only occur when there is an odd number of planes in the twin. Figure 5 shows a HREM image of an extrinsic faulted loop, which appears to cause nucleation of microtwins by superposition of extended faults in the neighboring planes. The presence of these defects in terms of ternary additions to TiAl will be discussed.[7]

References

1. J. M. Howe, U. Dahmen and R. Gronsky, Phil. Mag. (1987) 56, 31.
2. G. J. Mahon and J. M. Howe, Met. Trans. A (1990), in press.
3. J. M. Howe, D. P. Basile, M. K. Hatalis and N. Prabhu, Acta Cryst. (1988) A44, 449.
4. A. Ourmazd, D. W. Taylor, J. Cunningham and C. W. Tu, Phys. Rev. Lett. (1989) 62, 933.
5. R. Kilaas, Proc. Ann. E.M.S.A. Meeting (1987) 45, 66.
6. D. Shechtman, M. L. Blackburn and H. A. Lipsitt, Met. Trans. A (1974) 5, 1373.

7. This research was supported by AFOSR under Contract No. F49620-87-C-00017.

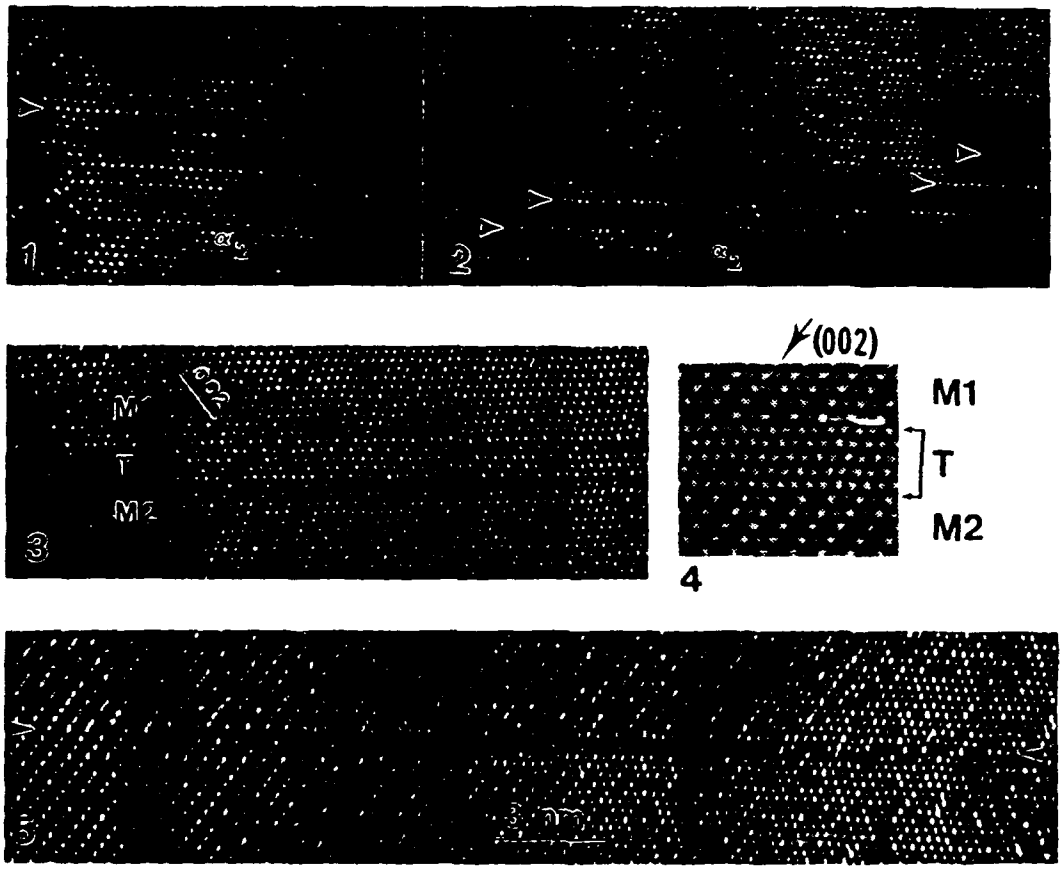

FIG. 1.--HREM image of $\gamma/\alpha 2$ interface in $<110]_\gamma$ orientation.
FIG. 2.--HREM image of $\gamma/\alpha 2$ interface in $<101]_\gamma$ orientation.
FIG. 3.--HREM image of twin interface in $<110]_\gamma$ orientation.
FIG. 4.--Simulated image of five plane twin with 1.9 mrad beam tilt.
FIG. 5.--HREM image of faulted loop.

Scripta METALLURGICA et MATERIALIA Vol. 24, pp. 2007-2012, 1990 Printed in the U.S.A.

ANALYTICAL ELECTRON MICROSCOPY OF COHERENT AND INCOHERENT $\alpha + \alpha_2$ PHASE EQUILIBRIA IN A Ti - 16.64 at% Al ALLOY

J. Y. Huh, J. M. Howe and William C. Johnson
Department of Metallurgical Engineering and Materials Science
Carnegie Mellon University
Pittsburgh, PA 15213-3890, USA

(Received August 13, 1990)

Introduction

A number of predictions have been made recently concerning phase equilibria in coherent solids [1-5]. These predictions indicate that equilibria in coherent systems can differ in fundamental ways from those of fluid or incoherent solid systems due to the existence of long-range stress fields. One characteristic of coherent phase equilibrium is that the phase boundaries, which delineate single-phase from two-phase fields, need not coincide with the tie-line ends that give the equilibrium compositions of the two coexisting phases. Indeed, in a temperature-composition phase diagram of a coherent system at constant external stress (pressure), the equilibrium phase compositions are functions of the bulk alloy composition. Furthermore, the equilibrium phase compositions are not confined to concentrations that lie within the two-phase incoherent phase field but may have concentrations that lie well within the single-phase fields [6,7]. Although the concentration shifts due to coherecy strain are predicted to be large enough to be measured, decisive experimental investigations designed to test these predictions have not been performed.

The main purpose of this note is to report initial experimental results comparing the equilibrium phase compositions of a two-phase coherent binary Ti-Al alloy with those of the corresponding incoherent alloy. Analytical electron microscopy (AEM) was used to determine phase compositions in both the coherent and incoherent equilibrium states. The two-phase field of $\alpha + \alpha_2$ in a Ti-Al binary alloy was chosen for this investigation for both theoretical and experimental reasons: (1) both the single-phase fields of α and α_2 have large composition ranges [8] which allow for significant composition shifts to offset elastic energy effects, (2) due to their relatively small misfit, the α_2 precipitates remain coherent up to sizes large enough to allow measurement of the composition by AEM, and (3) the α_2 precipitates have an ellipsoidal shape with an aspect ratio of about 4, so that they extend through the thin foil for compositional measurement. Because the equilibrated coherent α_2 precipitate is relatively small in size, usually less than 150 nm in diameter, the composition measurement can be most effectively performed by AEM.

Experimental Procedures

Sample Preparation

The alloy for this study was provided by RMI Co. in the form of a 50g button and was prepared by vacuum arc melting. Chemical analyses showed that the alloy contained 0.109 wt% oxygen and 0.121 wt% Fe. For all heat treatments, samples were wrapped in Ta foil and encapsulated in quartz tubes, which were evacuated to 10^{-6} torr and backfilled with purified Ar to 1/3 atm. At the end of each heat treatment, the samples were quenched in ice-water and the quartz capsules were broken immediately.

The as-received button was first homogenized in the single phase α region (1025 °C) for 50 hrs. The button was then cut into 1 cm cubes and aging treatments were performed at 800 °C. The aging temperature was controlled to within ±2 °C. Samples aged for 150 hrs yielded coherent precipitates. To obtain incoherent precipitates, (or, strictly speaking, semicoherent precipitates in which the misfit strains were completely relieved), samples were first aged at 800 °C for 124 hrs, cold rolled about 15 % and then aged an additional 1000 hrs at 800 °C. Because of possible segregation even after the homogenization treatment, alloy composition was determined by AEM in the areas where AEM analyses for phase compositions were performed. The alloy composition was 16.64 ± 0.25 at% Al and there was no significant difference between the coherent and incoherent alloy compositions. The alloy composition was measured in the same manner as the phase compositions, as discussed in the following sections.

Thin foils for AEM were prepared by electropolishing and then ion-milled for 20 min to remove any surface layer formed during electropolishing. Compositional analyses were performed in a Philips EM420T TEM/STEM equipped with a PGT+4 energy-dispersive x-ray (EDX) analyzer. A cold-stage holder was used to minimize contamination during the long exposure to the electron

0036-9748/90 $3.00 + .00

beam required to obtain adequate x-ray counting statistics. The STEM system was operated in 'μμD' mode because it was possible to obtain an image of the specimen on the TEM screen and place the electron probe on a small precipitate of interest more conveniently and more exactly than in the STEM mode. Care was taken to insure that the area of analysis was not in two-beam condition in order to prevent electron channeling effects [9]. The x-ray collection time was 200 sec and the electron-probe size was about 30 nm, which was measured directly from TEM negatives.

Absorption Correction and Error Estimation

The mass absorption coefficients for the Al-K_α peak are much larger than those for the Ti-K_α peak in Ti - Al alloys [10] Therefore, the analyzed composition in Ti-Al alloys can be affected by absorption even when conditions such as the setting of the electron microscope and the take-off angle are kept constant throughout the analysis. The x-ray data were analyzed by the absorption-correction method [11] as given by the following equations :

$$\frac{C_{Ti}}{C_{Al}} = k_{TiAl} \frac{I_{Ti}}{I_{Al}} \left\{ \frac{(\mu/\rho)^{Ti}_{Sp}}{(\mu/\rho)^{Al}_{Sp}} \right\} \left\{ \frac{1 - exp[-(\mu/\rho)^{Al}_{Sp}(\rho t)\, cosec\, \alpha]}{1 - exp[-(\mu/\rho)^{Ti}_{Sp}(\rho t)\, cosec\, \alpha]} \right\} \quad (1)$$

$$C_{Ti} + C_{Al} = 1 \quad (2)$$

where

$$(\mu/\rho)^{Ti}_{Sp} = C_{Ti}(\mu/\rho)^{Ti}_{Ti} + C_{Al}(\mu/\rho)^{Ti}_{Al} , \quad (3)$$

$$(\mu/\rho)^{Al}_{Sp} = C_{Ti}(\mu/\rho)^{Al}_{Ti} + C_{Al}(\mu/\rho)^{Al}_{Al} , \quad (4)$$

C_{Ti} and C_{Al} are the wt% of Ti and Al present at the point of analysis, I_{Ti} and I_{Al} are the intensities integrated in 1.2 FWHM (full width at half maximum) of the background-subtracted Ti-K_α and Al-K_α peaks, $(\mu/\rho)^A_B$ is the mass absorption coefficient of A-K_α in B element, and k_{TiAl} is a proportionality constant, often called the Cliff-Lorimer factor, which is estimated in the limit of a thin-film specimen. Before microanalysis, k_{TiAl} was determined from measurement on a standard sample with the exact chemical composition of Ti-15.88 wt% Al, which was homogenized at 1000 °C in the single phase (α_2) region. The value of k_{TiAl} was 1.05 ± 0.01 at a 99% confidence level. In order to use the above equations, it is necessary to know the foil thickness, t. There are various methods available for the measurement of foil thickness [12]. We used an indirect method in this study, the details of which are discussed in the following section.

The accuracy of the results obtained from Eqns. 1 and 2 is primarily limited by the counting statistics of the x-ray collection process [9,13]. Because the x-ray spectra were collected for sufficient time to obtain several thousand counts in each peak, the counting statistics can be assumed to follow a normal distribution. Since the composition of a phase is determined from n individual collections taken from different points ($22<n<43$ in this analysis), the confidence interval is estimated by the statistics of the student t-distribution or normal distribution (for $n>30$). The relative error, $\varepsilon_{I_{Ti}/I_{Al}}$, in I_{Ti}/I_{Al} at a 99% confidence level is given by the following equation:

$$\varepsilon_{I_{Ti}/I_{Al}} = \frac{100\, t_{99}\, S}{\sqrt{n}\,(I_{Ti}/I_{Al})_{Av}} \quad (5)$$

where $(I_{Ti}/I_{Al})_{Av}$ is the mean value calculated from n values of I_{Ti}/I_{Al}, t_{99} is the Student t value at a 99% confidence level, and S is the standard deviation.

The relative error, $\varepsilon_{C_{Ti}/C_{Al}}$, in $(C_{Ti}/C_{Al})_{Av}$ is the sum of $\varepsilon_{k_{TiAl}}$ and $\varepsilon_{I_{Ti}/I_{Al}}$, or

$$\varepsilon_{C_{Ti}/C_{Al}} = \varepsilon_{k_{TiAl}} + \varepsilon_{I_{Ti}/I_{Al}} \quad (6)$$

where $\varepsilon_{k_{TiAl}}$ is also determined by Eqn. 5. The relative error in the determination of C_{Al} for each phase was assumed to be equal to $\varepsilon_{C_{Ti}/C_{Al}}$.

Results and Discussion

Morphologies of Coherent and Incoherent (Semicoherent) States

In an alloy consisting of a dispersion of coherent particles within a matrix, the elastic field will be a strong function of position and simultaneously satisfying all equilibrium conditions may be difficult. In addition, the equilibrium concentration may be a function

of position within both phases. Owing to the relatively large precipitate sizes and long aging times employed in this study, subsequent changes in phase composition with time should be negligible so long as the precipitates remain coherent and retain an approximately ellipsoidal shape. The measured compositions herein are averages over the precipitate and matrix phases.

Figure 1 shows the α_2 precipitate morphologies in the coherent state and Fig. 2 shows similar precipitates in the incoherent state after rolling and subsequent aging. The coherent precipitates have a rod-like ellipsoidal shape with the major axis along the [0001] direction and an aspect ratio of about 4. The diameter of the precipitates shown in Fig. 1 is about 120 nm. This figure also shows the alignment of the particles along the [0001] direction. This alignment and the strong elastic strain-field contour in a two-beam condition indicate that the precipitates are under the influence of coherency stresses. Since elastic Ashby-Brown contrast [14] can still exist after a partial loss of coherency, complete coherency can be further verified by the observation of a lack of misfit dislocations in the precipitate interfaces. After aging for 150 hrs at 800 °C, misfit dislocations were observed only in several large precipitates at grain boundaries or low angle boundaries. However, our focus was on the matrix precipitates. The incoherent state displayed irregularly shaped precipitates which were wrapped by well-developed misfit dislocations as shown in Fig. 2. Thus, the coherency stresses were released and this state could be thought of as a state without any significant stress effect involved.

One of the important precautions which should be taken in quantitative x-ray microanalysis of a precipitate phase dispersed in a matrix is to ensure that the precipitate extends through the thickness of the foil. Otherwise, the collected x-ray spectrum will result from both the precipitate and matrix so that the exact composition of a precipitate cannot be determined. This could be overcome for both the coherent and semicoherent precipitates in this investigation. For the case of coherent precipitates, microanalyses were performed near a [0001] orientation, thereby ensuring that the precipitates extended through the foil. For the semi-coherent case with precipitates wrapped by well developed misfit dislocations, it was ensured from the cutting of the misfit dislocations by both foil surfaces, as shown in Fig. 2.

Quantitative X-ray Microanalysis

As mentioned previously, an indirect method was used to measure the foil thickness for absorption correction. If the absorption of the Ti-K_α peak in a thin-foil specimen is assumed to be negligible, the generated intensity of this characteristic peak is given by a simple formula [13]:

$$I_{Ti} = C \cdot C_{Ti}\, t \qquad (7)$$

where C is a proportionality constant for a consistent operating condition and t is the thickness in units of nm. Therefore, I_{Ti} is proportional to the foil thickness for a constant concentration of Ti. Figure 3 shows this linear relationship between I_{Ti} and t for the matrix in the incoherent sample, where the thickness was determined by the convergent-beam electron diffraction method. From this plot, the value of C was about 0.0415. However, Fig. 3 is for a slightly different operating condition than that used for the subsequent quantitative microanalysis, i.e., a larger spot size (electron probe) was used for Fig. 3 than in the analyses. This changes the electron-beam current. Therefore, the proportionality constant, C, for the operating condition used in the microanalyses was estimated to be about 0.015 from the ratio between two I_{Ti} collected from an identical area at the two operating conditions. In principle, the composition analysis for a foil with unknown composition must be calculated systematically by the iteration method after substituting Eqn. 7 into Eqn. 1. In our analysis, 90.96 wt% (85 at%) was used for C_{Ti} in Eqn. 7 as well as in Eqn. 3 and Eqn. 4 for the matrix, and 87.77 wt% (80 at%) was used for the precipitate analyses. This may alter the absolute values of the resulting compositions slightly, but its effect should be so small as to be negligible compared to other sources causing errors, particularly estimation of the proportionality constant C. A direct determination of C for the operating condition used would be necessary to increase the reliability of the absolute value of the measured composition. However, the method discussed above should be sufficiently accurate to identify the difference between absolute compositions, i.e., the difference between the compositions of matrix (or precipitate) in coherent and incoherent states, because the compositions in both states were measured in a similar range of thickness, as shown in Fig. 4. Therefore, the error in absorption correction was assumed to be negligible compared with the counting statistics errors in k_{TiAl} and $(I_{Ti}/I_{Al})_{Av}$.

The results of the AEM analyses are shown in Fig. 4, where the distribution of data about the average composition with respect to the number of counts in the Ti-K_α peak (corresponding to thickness) are also indicated. The matrix and precipitate compositions in the coherent state are 14.15 ± 0.32 and 19.80 ± 0.61 at% Al, respectively, and those in the incoherent state are 14.79 ± 0.32 and 20.82 ± 0.42 at% Al, respectively. Both phase compositions are shifted to the Ti-rich side under coherency stresses although the error bars estimated at the 99% confidence level do touch one another in the matrix. The significance of the shifts in phase compositions under coherency stresses can be tested statistically to find the value of t for making small-sample inference about the difference between two true compositions [15]. When C and S are, respectively, the average composition and standard deviation for n measurements for a phase in the incoherent and coherent states designated by the subscripts inc and co, respectively, t can be determined by:

$$t = \frac{C_{unc} - C_{co}}{\sqrt{S_p^2 \left(1/n_{unc} + 1/n_{co} \right)}} \qquad (5)$$

where

$$S_p^2 = \frac{(n_{unc} - 1) S_{unc}^2 + (n_{co} - 1) S_{co}^2}{n_{unc} + n_{co} - 2} \qquad (6)$$

If the absolute value of t is greater than 2.8, the shift can be concluded to be sufficiently significant at a 99% confidence level. The values for the shifts in both the matrix and precipitate compositions in these microanalyses are greater than 3.5. Therefore, we conclude that there are definite shifts in both matrix and precipitate compositions to the Ti-rich side under the influence of coherency stresses. Since the phase boundaries of two-phase coexistence in a coherent system must lie inside those of an incoherent system, the results provide direct confirmation for the theoretical prediction that the tie-line ends are different from the phase boundaries in coherent equilibria. In this case, the concentration shift appears to be greater for the precipitate than for the matrix phase.

The decrease in spatial resolution due to beam spreading can affect quantitative x-ray microanalysis, especially for a small coherent precipitate. Since the width of the matrix in between precipitates is comparable to the precipitate diameter as shown in Fig. 1(a), beam spreading could potentially affect the microanalyses results from both phases. However, the measured compositions indicate that this effect is negligible, since the measured composition of Al in the matrix phase in the coherent state where the matrix is narrow is less than in the incoherent state where it is wide. This fact makes the analyzed compositions even more convincing.

Figure 5 shows a comparision of the results of this work with other studies conducted on Ti-Al alloys. The phase diagrams of both Blackburn [16] and Lutjering *et al.* [17], were determined by direct TEM observation of a series of alloys which had undergone prolonged aging at various temperatures. These results can be viewed as incoherent phase boundaries because the latter, who gave only the α / $\alpha+\alpha_2$ phase boundary, focused primarily on heterogeneous precipitation along grain boundaries. The results of Blackburn and Lutjering *et al.* are in good agreement with the incoherent compositions of the present work at 800 °C. On the other hand, the phase diagram of Swartzendruber *et al.* [18] was determined by magnetic susceptibility measurements to form the tie-line ends, and then by assuming implicitly that the tie-line ends coincided with the phase boundaries. Their α / $\alpha+\alpha_2$ boundary was significantly shifted to the Ti-rich region compared with those of Blackburn and Lutjering *et al.*, even considering their estimated error of 1 at%. This shift is consistent with our result of the shift in matrix composition under coherency stresses, although a quantative comparison may not be possible even at 800 °C due to the fact that they used a different alloy composition (20 at% Al for 800 °C). From their micrograph and aging treatments, we feel that the α_2 precipitates are mostly coherent and under the influence of coherency stresses. Thus, we believe that the results of Swartzendruber *et al.* [18] should be interpreted as tie-line ends rather than as phase boundaries. As for the $\alpha+\alpha_2$ / α_2 phase boundary, our result does not agree with that of Ref [18] (which is apparently shifted to α_2 single-phase field with respect to that of Ref [16] throughout the two-phase region). The reason for this is not fully understood at this point. However, we believe that some of the disagreement in the literature concerning the $\alpha + \alpha_2$ region in the Ti - Al phase diagram could be due to coherency effects.

In order to check whether or not the phase compositions are functions of bulk composition in coherent equilibria, additional experiments are now in progress.

Conclusions

The phase compositions in a Ti - 16.64 at% Al alloy aged in the $\alpha + \alpha_2$ region at 800 °C were determined for both the coherent and incoherent states by analytical electron microscopy. The compositions of the coexisting α (matrix) and α_2 (precipitate) phases in the coherent state were 14.15 ± 0.32 and 19.80 ± 0.61 at% Al, respectively, and those in the incoherent state were 14.79 ± 0.32 and 20.82 ± 0.42 at% Al, respectively. Both the matrix and precipitate compositions were shifted to the Ti-rich side of the phase diagram as a result of coherency stresses. The equilibrium composition of the matrix in the coherent state lies well within the single-phase field. These statistically significant results provide direct experimental evidence that, for a binary alloy in coherent equilibrium under constant external pressure, tie-line ends and phase boundaries are not coincident when viewed from a temperature-composition diagram.

Acknowledgements

We are grateful to D. B. Williams for several helpful suggestions regarding the AEM analyses. The authors gratefully acknowledge the financial support of the National Science Foundation through grants DMR-8620026 (JYH and WCJ) and DMR-8915770 (JMH) and partial support by the Air Force Office of Scientific Research through grant F49620-87-C-00017 (JMH).

References

1. R. O. Williams, CALPHAD 8, 1 (1984).
2. J. W. Cahn and F. C. Larche, Acta Metall. 32, 1915 (1984).
3. A. L. Roitburd, Sov. Phys. Solid State 26, 1229 (1984).
4. W. C. Johnson and P. W. Voorhees, Met. Trans. 18A, 1213 (1987).
5. W. C. Johnson and W. H. Muller, Acta Metall., in press.
6. C. S. Chiang and W. C. Johnson, J. Mat. Res. 4, 678 (1989).
7. Z. K. Liu and J. Agren, Acta Metall. 38, 561 (1990).
8. J. C. Mishurda, J. C. Lin, Y. A. Chang, and J. H. Perepezko, Mat. Res. Soc. Symp. Proc. 133, ed., C. T. Liu, A. I. Taub, N. S. Stoloff, and C. C. Koch, 57 (1989).
9. J. I. Goldstein, D. B. Williams, C. E. Fiori, and G. Cliff, in "Principles of Analytical Electron Microscopy", ed., D. C. Joy, A. D. Romig, Jr. and J. I. Goldstein, Plenum Press, New York, Chapters 4 and 5 (1986).
10. K. F. J. Heinrich, in "The Electron Microprobe", ed., T. D. McKinley, K. F. J. Heinrich, and D. B. Wittry, J. Wiley, NY, 351 (1966).
11. J. I. Goldstein, J. L. Costley, G. W. Lorimer, and S. J. B. Reed, Scanning Electron Microscopy 1, ed., O. Johari, Chicago, IL, 315 (1977).
12. Z. Horita, K. Ichitani, T. Sano, and M. Nemoto, Phil. Mag. 59A, 939 (1988).
13. D. B. Williams, "Practical Analytical Electron Microscopy in Materials Science", Philips Electron Optics Publishing Group, Mahwah, NJ, Chapter 4 (1984).
14. M. F. Ashby and L. M. Brown, Phil. Mag. 8, 1649 (1963).
15. J. T. McClave and F. H. Dietrich, II, in "Statistics", 3rd ed., Collier Macmillan, London, Chapter 8 (1985).
16. M. J. Blackburn, Trans. Metall. Soc. AIME 239, 1200 (1967).
17. G. Lutjering and S. Weissmann, Acta Metall. 18, 785 (1970).
18. L. J. Swartzendruber, L. H. Bennett, L. K. Ives, and R. D. Shull, Mat. Sci. Eng. 51, p1 (1981).

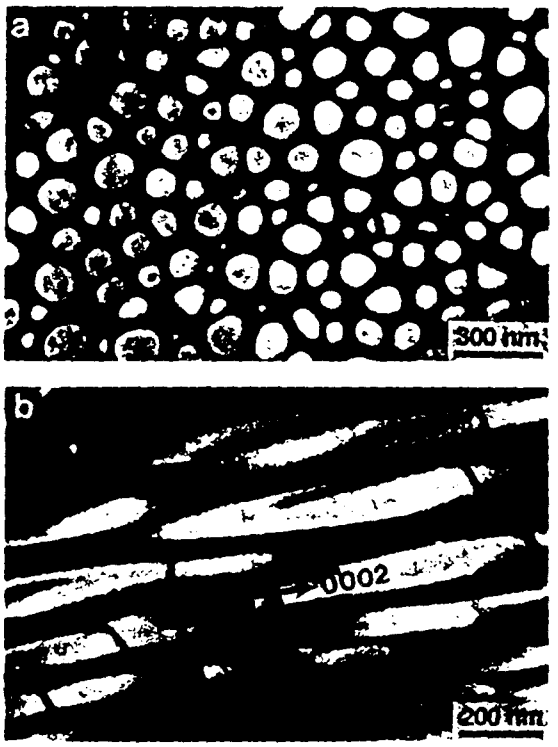

Fig. 1. Coherent precipitates in aged Ti - 16.64 at% Al ; 150 hrs 800 °C. Dark field using precipitate reflection. (a) Zone normal [0001]. (b) Zone normal [1210]. Note alignment of precipitates along [0001] and cylinder-like morphology of precipitates.

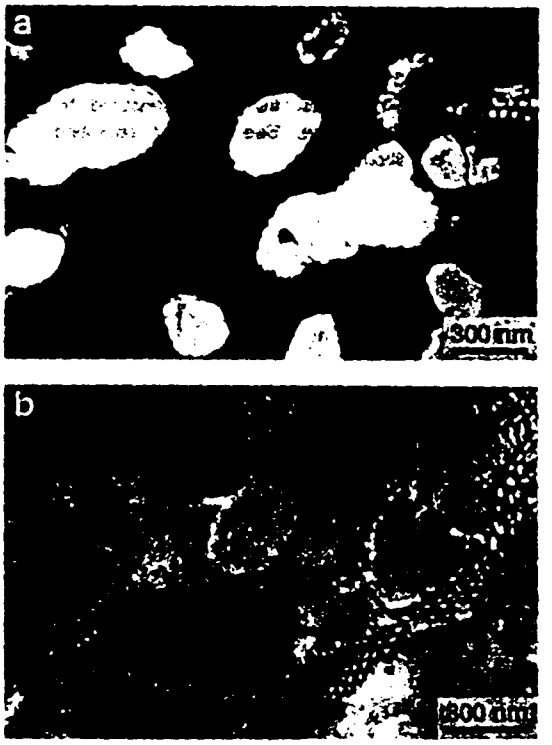

Fig. 2. Semicoherent precipitates in deformed and aged Ti - 16.64 at% Al ; 124 hrs 800 °C + rolling + 1000 hrs 800 °C. (a) Zone normal [0001]. Note irregular shape of precipitate. (b) Zone normal [0001] and same area as (a). Note well developed misfit dislocations.

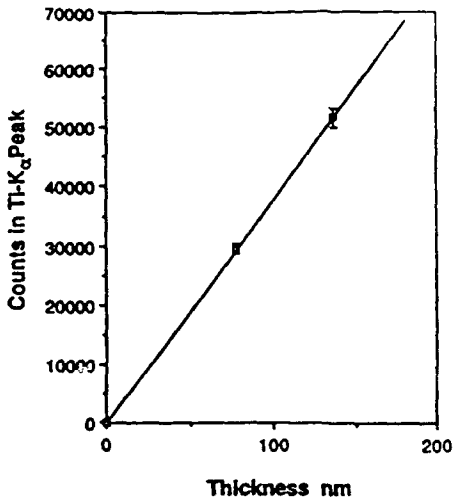

Fig. 3. Integrated counts of Ti - K_α peak in 1.2 FWHM vs. thickness measured by CBED method. See text for operating condition used.

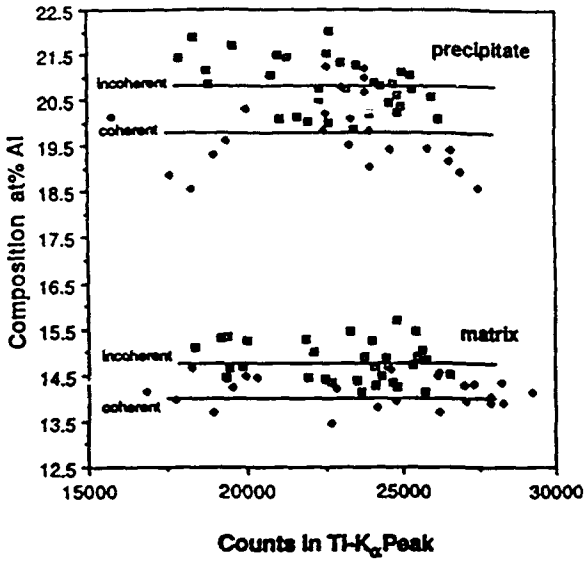

Fig. 4. Data distributions for both coherent (filled square) and incoherent (square) states in Ti - 16.64 at% Al aged at 800 °C. The absorption effect due to the thickness variation among data was corrected. Horizontal lines are average compositions.

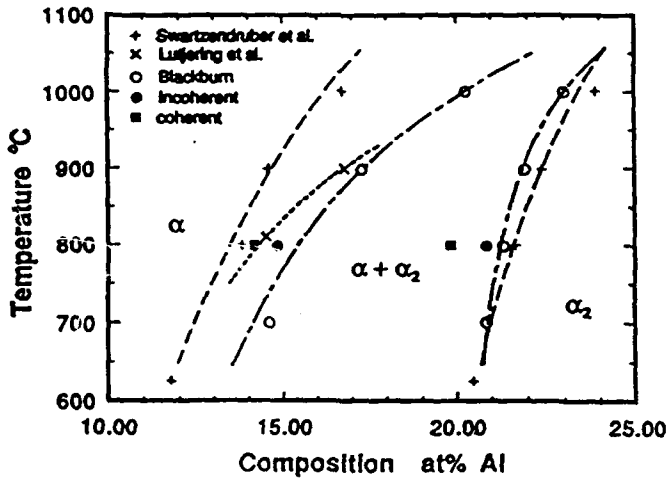

Fig. 5. A comparision of the results of the present work with the phase diagrams of Blackburn [16], Lutjering *et al.* [17] and Swartzendruber *et al.* [18].